

## Phenomenology of GUT-less Supersymmetry Breaking

John Ellis<sup>1</sup>, Keith A. Olive<sup>2</sup> and Pearl Sandick<sup>2</sup>

<sup>1</sup>*TH Division, PH Department, CERN, CH-1211 Geneva 23, Switzerland*

<sup>2</sup>*William I. Fine Theoretical Physics Institute,  
University of Minnesota, Minneapolis, MN 55455, USA*

### Abstract

We study models in which supersymmetry breaking appears at an intermediate scale,  $M_{in}$ , below the GUT scale. We assume that the soft supersymmetry-breaking parameters of the MSSM are universal at  $M_{in}$ , and analyze the morphology of the constraints from cosmology and collider experiments on the allowed regions of parameter space as  $M_{in}$  is reduced from the GUT scale. We present separate analyses of the  $(m_{1/2}, m_0)$  planes for  $\tan\beta = 10$  and  $\tan\beta = 50$ , as well as a discussion of non-zero trilinear couplings,  $A_0$ . Specific scenarios where the gaugino and scalar masses appear to be universal below the GUT scale have been found in mirage-mediation models, which we also address here. We demand that the lightest neutralino be the LSP, and that the relic neutralino density not conflict with measurements by WMAP and other observations. At moderate values of  $M_{in}$ , we find that the allowed regions of the  $(m_{1/2}, m_0)$  plane are squeezed by the requirements of electroweak symmetry breaking and that the lightest neutralino be the LSP, whereas the constraint on the relic density is less severe. At very low  $M_{in}$ , the electroweak vacuum conditions become the dominant constraint, and a secondary source of astrophysical cold dark matter would be necessary to explain the measured relic density for nearly all values of the soft SUSY-breaking parameters and  $\tan\beta$ . We calculate the neutralino-nucleon cross sections for viable scenarios and compare them with the present and projected limits from direct dark matter searches.

April 2007

# 1 Introduction

Over the past three and a half decades, the Standard Model (SM) of particle physics has been remarkably successful at describing the interactions of elementary particles at or below the weak scale. However, there are several compelling reasons to expect that the SM is merely a low-energy effective theory that fits into a larger framework. Chief among these reasons are the related hierarchy and naturalness problems, namely the creation and maintenance of a large hierarchy of mass scales despite the fact that the electroweak Higgs potential is unstable with respect to quantum corrections within the SM [1]. The appearance of supersymmetry (SUSY) at the TeV scale would not only solve the naturalness problem and facilitate the unification of gauge couplings at a high scale as in simple Grand Unified Theories (GUTs) [2], but also predict a light Higgs boson as apparently favoured by the high-precision electroweak data [3]. With the additional plausible assumption of R-parity conservation, the lightest SUSY particle (LSP) is stable and, if uncharged, is a natural candidate for astrophysical cold dark matter [4]. For these reasons, models with SUSY broken at the TeV scale are extensively studied.

It is evident that SUSY must be broken, since we have not yet observed any superpartners of SM particles, but the mechanism of SUSY breaking and how this breaking is communicated to the observable sector have been the subjects of much speculation [5]. Phenomenologically, the magnitudes of the SUSY-breaking parameters observable at low energies are often calculated by assuming values of the soft SUSY-breaking parameters at some high input scale and evolving them down to lower scales using the renormalization-group equations (RGEs) of the effective low-energy theory. This is generally taken to be the minimal supersymmetric extension of the SM (MSSM) [6]. In the constrained MSSM (CMSSM) [7–13], the soft SUSY-breaking parameters are assumed to be universal at the high scale. It should be noted, however, that there are many theories of SUSY breaking in which the soft SUSY-breaking parameters are not universal at the input scale [14].

The CMSSM can be parametrized at the universality scale by five free input parameters, namely the scalar mass,  $m_0$ , the gaugino mass,  $m_{1/2}$ , the trilinear soft breaking parameter,  $A_0$ , the ratio of the Higgs vevs,  $\tan\beta$ , and the sign of the Higgs mass parameter,  $\mu$ . The input scale at which universality is assumed in CMSSM models is usually taken to be the SUSY GUT scale,  $M_{GUT} \sim 2 \times 10^{16}$  GeV. However, it may be more appropriate in some models to assume the soft SUSY-breaking parameters to be universal at some different input scale,  $M_{in}$ , which may either be intermediate between  $M_{GUT}$  and the electroweak scale [15], the case studied here, or perhaps larger than  $M_{GUT}$  [16].

Specific scenarios in which the soft SUSY-breaking parameters may be universal at a scale below  $M_{GUT}$  occur in models with mixed modulus-anomaly mediated SUSY breaking (MM-AMSB), also called mirage-mediation [17], and models with warped extra dimensions [18]. In the case of mirage-mediation, the universality scale is the mirage messenger scale, which is predicted to be  $M_{in} \sim 10^{10} - 10^{12}$  GeV in the case of KKLT-style moduli stabilization [19]. In other models, the universality scale may lie anywhere between 1 TeV and  $M_{Pl}$ .

In this paper, we present an in-depth study of the effect on the allowed regions of the CMSSM parameter space of lowering the assumed universality scale. We focus on the de-

pendences of the constraints from cosmology and collider experiments on the value of  $M_{in}$  in such GUT-less scenarios, paying particular attention to the regions of parameter space favored by the value of the cold dark matter relic density inferred from WMAP [20] and other measurements, assuming that the cold dark matter is mainly provided by the lightest neutralino  $\chi$ . Within the GUT-less allowed regions, we also calculate the neutralino-nucleon cross sections and compare them with present and expected limits from direct searches for cold dark matter.

This work is a sequel to the exploratory study of GUT-less CMSSM scenarios made in [15], in which our attention was restricted to the case  $\tan\beta = 10$ ,  $A_0 = 0$ ,  $\mu \geq 0$  and  $M_{in} \geq 10^{11.5}$  GeV. We found that, as the universality scale was reduced to this value, one of the most dramatic changes was to the footprint in the  $(m_{1/2}, m_0)$  plane of the constraint on the relic abundance of neutralinos inferred from WMAP *et al.* In the standard GUT-scale universality case, there are three well-defined cosmologically preferred regions of parameter space where the relic density of neutralinos matches the estimate of the cold dark matter relic density based on data from WMAP and other observations: the coannihilation region [21], the rapid-annihilation funnel [9,22] and the focus-point region [23]. In the GUT-less CMSSM scenario [15], we found that, as the universality scale is lowered to  $M_{in} \sim 10^{12}$  GeV, these regions approach and merge, forming a small WMAP-preferred island in a sea of parameter space where the neutralino relic density is too small to provide all the cold dark matter wanted by WMAP. We found that, in this case, the only region with a neutralino relic density that exceeds the WMAP measurement is a ‘vee’ at large  $m_{1/2}$ , bordering the region where the stau is the LSP.

In this paper, we extend the previous analysis to include other values of  $A_0$  for  $\tan\beta = 10$ , to the case  $\tan\beta = 50$ , and to lower values of  $M_{in}$ . For this purpose, we extend the code used previously to evaluate the cold dark matter density by implementing all coannihilations between the three lightest neutralinos and the lighter chargino species. As we exhibit explicitly, their inclusion is essential for an accurate calculation of the relic density in some important regions of the GUT-less parameter space. The second objective of this paper is to calculate the neutralino dark matter scattering cross sections (both spin-dependent and spin-independent) in such GUT-less models.

The outline of the paper is as follows. In Section 2 we discuss briefly the renormalizations of the SUSY-breaking contributions to the masses of the squarks, sleptons and gauginos as functions of  $M_{in}$ , as a preliminary to provide background understanding for some of the results presented later. Then, in Section 3 we discuss the current experimental, phenomenological and cosmological constraints on CMSSM scenarios that we use. Section 4 contains our core discussion of the variation in the allowed region of parameter space as  $M_{in}$  is decreased from the GUT scale down to  $M_{in} = 10^9$  GeV, for both  $\tan\beta = 10$  and  $\tan\beta = 50$ . We also present a separate treatment of the mirage-mediation scenario [17] with KKLT moduli stabilization [19]. We then present in Section 5 the corresponding predictions for neutralino-nucleon scattering cross sections in GUT-less scenarios, and Section 6 summarizes our conclusions. An Appendix motivates and discusses relevant details of our implementation of multi-channel neutralino and chargino coannihilation.

## 2 Renormalization of SUSY-Breaking Mass Parameters

In order to understand the changes in the allowed regions in the  $(m_{1/2}, m_0)$  plane of the CMSSM that occur as  $M_{in}$  is lowered, it is necessary first to understand the consequences for the observable sparticle masses of lowering the universality scale. In the CMSSM with universality imposed at the GUT scale, the one-loop renormalizations of the gaugino masses  $M_a$ , where  $a = 1, 2, 3$ , are the same as those for the corresponding gauge couplings,  $\alpha_a$ . Thus, at the one-loop level the gaugino masses at any scale  $Q \leq M_{GUT}$  can be expressed as

$$M_a(Q) = \frac{\alpha_a(Q)}{\alpha_a(M_{GUT})} M_a(M_{GUT}), \quad (1)$$

where  $M_a(M_{GUT}) = m_{1/2}$ . On the other hand, in a GUT-less CMSSM, where the gauge-coupling strengths run at all scales below the GUT scale but the soft SUSY-breaking parameters run only below the lower universality scale,  $M_{in}$ , at which all the gaugino masses are assumed to be equal to  $m_{1/2} = M_a(M_{in})$ , we have

$$M_a(Q) = \frac{\alpha_a(Q)}{\alpha_a(M_{in})} m_{1/2} \quad (2)$$

at the one-loop level. Since the runnings of the coupling strengths in GUT and GUT-less CMSSM scenarios are identical, the low-energy effective soft gaugino masses,  $M_a(Q)$ , in GUT-less cases are less separated and closer to  $m_{1/2}$  than in the usual GUT CMSSM, as seen explicitly in panel (a) of Fig. 1<sup>1</sup>.

The soft SUSY-breaking scalar masses are renormalized by both gauge and (particularly in the cases of third-generation sfermions) Yukawa interactions, so the running is somewhat more complicated. At the one-loop level one can summarize the effects of renormalizations at any  $Q \leq M_{in}$  as

$$m_{0_i}^2(Q) = m_0^2(M_{in}) + C_i(Q, M_{in}) m_{1/2}^2, \quad (3)$$

where we make the CMSSM assumption that the  $m_0^2(M_{in})$  are universal at  $M_{in}$ , and the  $C_i(Q, M_{in})$  are renormalization coefficients that vanish as  $Q \rightarrow M_{in}$ . We display in panels (b) and (c) of Fig. 1 the two-loop-renormalized soft SUSY-breaking masses of the first- and second-generation left- and right-handed squarks,  $\tilde{q}_{L,R}$ , the stop mass eigenstates,  $\tilde{t}_{1,2}$ , and the left- and right-handed sleptons,  $\tilde{\ell}_{L,R}$ . We see again that in GUT-less cases the soft SUSY-breaking scalar masses are less separated and closer to  $m_0$  than in the usual GUT-scale CMSSM.

In the CMSSM, the electroweak vacuum conditions are used to fix the values of  $|\mu|$  and  $m_A$ . Although we use the full two-loop renormalizations, insight into the effects of

---

<sup>1</sup>Note that in making this plot we have included the full two-loop renormalization-group equations for the gaugino masses, which are not identical to those for the gauge couplings, although the difference is not very striking.

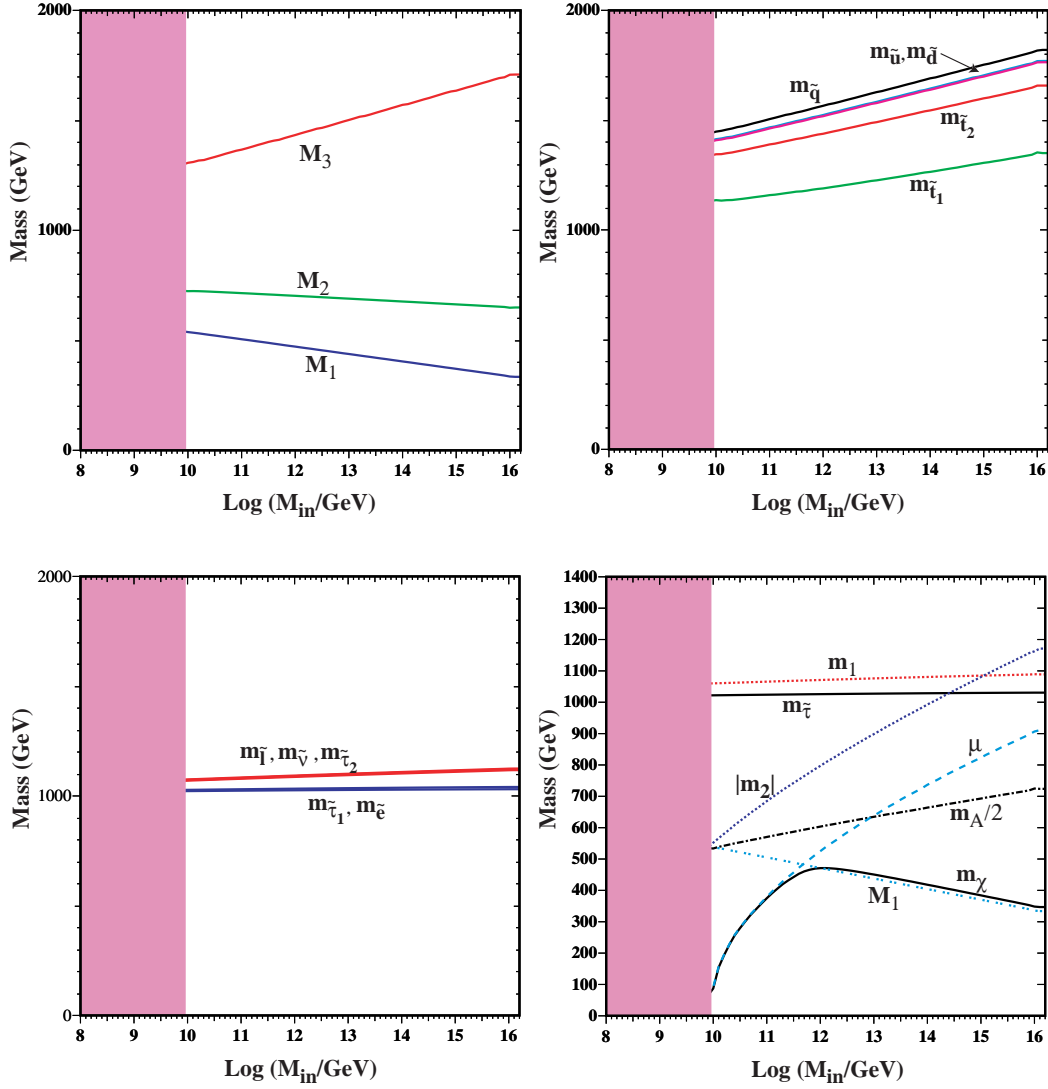


Figure 1: The dependences of observable sparticle mass parameters on the input scale  $M_{in}$  at which they are assumed to be universal: (a) gaugino masses  $M_{1,2,3}$ , (b) squark masses, (c) slepton masses, and (d) Higgs ( $m_{1,2}, m_A$ ), stau and the lightest neutralino  $\chi$  masses, as well as  $\mu$  and the  $U(1)$  gaugino mass  $M_1$ . The calculations are made for the representative case  $m_{1/2} = 800 \text{ GeV}$ ,  $m_0 = 1000 \text{ GeV}$ ,  $A_0 = 0$ ,  $\tan\beta = 10$  and  $\mu > 0$ .

varying  $M_{in}$  on the required values of  $|\mu|$  and  $m_A$  can be gleaned from simple leading-order expressions. The tree-level solution for  $\mu$  is

$$\mu^2 = \frac{m_1^2 - m_2^2 \tan^2 \beta}{\tan^2 \beta - 1} - \frac{M_Z^2}{2}, \quad (4)$$

where  $m_1$  and  $m_2$  are the soft Higgs masses associated with  $H_1$  and  $H_2$ , respectively. The variation of  $\mu$  with  $M_{in}$  for one fixed pair of values of  $(m_{1/2}, m_0)$  is seen in panel (d) of Fig. 1, where we see that the solution of (4) for  $\mu^2$  becomes negative and unphysical for  $M_{in} < 10^{10}$  GeV. For this value of  $M_{in}$ , values of  $m_0 > 1000$  GeV would not yield physical electroweak vacua. One can see from (3) and panels (b) and (c) of Fig. 1 that, as  $M_{in}$  decreases, the soft scalar masses remain closer to the input value,  $m_0$ . This has the converse result that, for any fixed  $m_{1/2}$ , as the universality scale is lowered,  $\mu^2$  changes sign and becomes unphysical at smaller values of  $m_0$ , causing the upper boundary of the unphysical region to creep down farther into the  $(m_{1/2}, m_0)$  plane. This explains the encroachment of the upper-left excluded regions in the  $(m_{1/2}, m_0)$  planes shown later in Figures 2 - 5, as  $M_{in}$  decreases.

The weak-scale value of  $m_A$  decreases with  $M_{in}$  logarithmically, as also seen in panel (d) of Fig. 1, and also in panels (c) and (d) of Fig. 3 of [15]. In addition to its importance for the direct detection of the near-degenerate  $A, H$  and  $H^\pm$  bosons, this feature is important indirectly for several aspects of our later discussion. One is the constraints from heavy-flavour physics to be discussed in the next section: since  $b \rightarrow s\gamma$  and  $B_s \rightarrow \mu^+ \mu^-$  at large  $\tan \beta$  have important contributions from the exchanges of heavier Higgs bosons, the impact of these constraints increases as  $m_A$  decreases and hence as  $M_{in}$  decreases. A second impact of  $m_A$  is on the cold dark matter density: since a rapid-annihilation funnel appears when  $m_\chi \simeq m_A/2$ , for fixed values of the other parameters such as  $\tan \beta, m_0$  and  $A_0$ , this funnel appears at lower  $m_\chi$  and hence  $m_{1/2}$  as  $M_{in}$  decreases. Finally, another potential impact is on the spin-independent neutralino dark-matter scattering cross section, which receives a significant contribution from heavy Higgs exchange, as discussed later.

In addition to the excluded regions in the upper left corners of each of the  $(m_{1/2}, m_0)$  planes shown in Figures 2-5 where electroweak symmetry breaking is not obtained, we see a second major excluded region in the lower right corner of each panel. In these regions of the plane, the lightest stau,  $\tilde{\tau}_1$ , becomes lighter than the lightest neutralino, resulting in a charged LSP, which is incompatible with general arguments from astrophysics and cosmology. As we see from (3), as  $M_{in}$  decreases the positive coefficient  $C_{\tilde{\tau}_1}$  also decreases because  $M_{in}$  is approaching the low scale,  $Q$ . Hence  $m_{\tilde{\tau}_1}$  gets progressively closer to  $m_0$  for any fixed  $m_{1/2}$ , as seen in panel (c) of Fig. 1. At the same time, the gaugino masses remain closer to  $m_{1/2}$  as  $M_{in}$  decreases, implying that, as long as the lightest neutralino remains essentially a bino, its mass becomes a larger portion of the universal gaugino mass. This can be seen in panel (d) of Fig. 1, where for this particular point in the  $(m_{1/2}, m_0)$  plane, the LSP mass tracks that of the bino for  $M_{in} \gtrsim 10^{12}$  GeV. As a result, for fixed  $m_{1/2}$  and  $m_0$ , as the universality scale  $M_{in}$  is lowered from  $M_{GUT}$ , initially  $m_{\chi_1}$  increases and  $m_{\tilde{\tau}_1}$  decreases. Hence, as  $M_{in}$  decreases for any fixed  $m_{1/2}$ , a larger value of  $m_0$  is required to enforce the condition  $m_{\chi_1} \leq m_{\tilde{\tau}_1}$ . For this reason, the lower-right excluded regions in the  $(m_{1/2}, m_0)$  planes shown in Figures 2 - 5 initially expand as  $M_{in}$  decreases.

However, since  $|\mu|$  decreases as  $M_{in}$  decreases, as discussed above, below a certain value of  $M_{in}$ ,  $|\mu|$  becomes small enough that the lighter Higgsino takes over as the LSP, with a mass that decreases as  $|\mu|$  continues to decrease. In panel (d) of Fig. 1, one can see that, for  $M_{in} \lesssim 10^{11}$  GeV, the LSP is sufficiently Higgsino-like that its mass is nearly identical to  $|\mu|$ . Since the boundary of the disallowed stau LSP region is determined by equality between the masses of the stau and the lightest neutralino, this boundary therefore falls to lower  $m_0$  when  $M_{in}$  is decreased below the bino-Higgsino cross-over point, as is seen in the  $(m_{1/2}, m_0)$  planes shown later in Figures 2 - 5.

### 3 Experimental, Phenomenological and Cosmological Constraints

Our treatments of experimental, phenomenological and cosmological constraints essentially follow those in [15], but with differences that we describe below.

#### 3.1 LEP Experimental Constraints

The appropriate LEP lower limit on the chargino mass for the class of CMSSM models discussed here is  $m_{\chi^\pm} > 104$  GeV [24], and the nominal effective lower limit on the mass of the lightest Higgs boson  $h$  is 114 GeV <sup>2</sup> [25]. However, in addition to displaying the direct position of the 114 GeV bound in the GUT-less parameter space, we also calculate and display the 95% CL limit obtained by combining the experimental likelihood,  $\mathcal{L}_{exp}$ , from direct searches at LEP 2 and a global electroweak fit, convolved with the theoretical and parametric errors in  $m_h$  <sup>3</sup>, which provides a more exact (and relaxed) interpretation of the LEP Higgs limit within the MSSM. The top mass used in these calculations is  $m_t = 171.4 \pm 2.1$  GeV [26].

We note that one can use (3) to predict how the impact of the LEP Higgs mass constraint varies with  $M_{in}$ . We recall that the mass of the lightest scalar MSSM Higgs boson  $m_h < M_Z$  at tree level, but is renormalized by an amount that depends logarithmically on  $m_{\tilde{t}}$ . Eq. (3) shows that  $m_{\tilde{t}}$  decreases as  $M_{in}$  is lowered for any fixed  $m_{1/2}$  and  $m_0$ . However,  $m_{\tilde{t}}$  also increases with  $m_{1/2}$ . Thus, one should expect that the LEP Higgs constraint moves to larger  $m_{1/2}$  as the universality scale is lowered.

#### 3.2 Muon Anomalous Magnetic Moment

It is well known that the measurement by the BNL g-2 Collaboration [28] disagrees significantly with the Standard Model if  $e^+e^-$  annihilation data are used to calculate the Standard

---

<sup>2</sup>We implement this constraint by calculating the lightest Higgs mass with the previous version of the FEYNHIGGS code [27], which incorporates a direct interface with the underlying CMSSM parameters, and allowing a possible error of 1.5 GeV to account for possible higher-order contributions. We have verified that the numerical difference from the more recent version of FEYNHIGGS is considerably smaller than our error allowance.

<sup>3</sup> We thank A. Read for providing the LEP  $CL_s$  values.

Model contribution, but there is no significant discrepancy if this is calculated using  $\tau$ -decay data [29]. In view of the lack of consensus on the interpretation of the measurement of  $a_\mu = (g_\mu - 2)/2$ , we use it only as part of our motivation for restricting our study to the case  $\mu > 0$ . However, if the  $e^+e^-$  estimate of the hadronic contribution to the Standard Model calculation is accepted, one finds [30]:

$$a_\mu(\text{theory}) = (11659180.5 \pm 5.6) \times 10^{-10}, \quad (5)$$

$$a_\mu(\text{experiment}) = (11659208.0 \pm 6.3) \times 10^{-10}, \quad (6)$$

yielding a discrepancy [29]

$$\Delta a_\mu = (27.5 \pm 8.4) \times 10^{-10}, \quad (7)$$

which would be a  $3.3\text{-}\sigma$  effect. In the plots discussed later, we display the corresponding  $2\text{-}\sigma$  range, namely

$$10.7 \times 10^{-10} < \Delta a_\mu < 44.3 \times 10^{-10}. \quad (8)$$

### 3.3 B Decay Observables

We consider two constraints provided by B decay: one is the agreement between experiment and theory for  $b \rightarrow s\gamma$  [31], and the other is the experimental upper limit on  $B_s \rightarrow \mu^+ \mu^-$  decay. The recent measurements of  $B^\pm \rightarrow \tau^\pm \nu$  decay do not yet impinge significantly on the parameter space we explore in this paper.

In the case of  $b \rightarrow s\gamma$ , we use the estimate  $BR(b \rightarrow s\gamma) = (3.15 \pm 0.23) \times 10^{-4}$  [32] for the SM contribution at NNLO <sup>4</sup>, and the code of Gambino and Ganis <sup>5</sup> to calculate the MSSM contribution to the decay amplitude at NLO in QCD. As for the present experimental rate for  $b \rightarrow s\gamma$  decay, we use the range

$$BR(b \rightarrow s\gamma) = (3.55 \pm 0.24_{-0.13}^{+0.12}) \times 10^{-4} \quad (9)$$

as recommended by the HFAG [33, 34]. The first of the errors in (9) is the combined statistical and systematic experimental error. The second set of errors result from theoretical uncertainties and corrections. These are combined linearly with the scale uncertainty in the calculation. We recall that  $b \rightarrow s\gamma$  joins  $a_\mu$  in disfavouring  $\mu < 0$ .

In the case of  $B_s \rightarrow \mu^+ \mu^-$  decay, we calculate the rate in the MSSM using [35, 36], and we use the experimental upper limit

$$BR(B_s \rightarrow \mu^+ \mu^-) < 1.0 \times 10^{-7} \quad (10)$$

reported by CDF [37]. We also display in Figures 4 - 5 projected future sensitivities of the Tevatron and LHC experiments (a factor of 5 times lower than the current limit). As already noted, the the impact of the  $B_s \rightarrow \mu^+ \mu^-$  constraint is important at large  $\tan \beta$ , and increases as  $m_A$  decreases and hence as  $M_{in}$  decreases.

---

<sup>4</sup>We note that the dominant theoretical error due to the renormalization-scale uncertainty it is not Gaussian, and hence we add it linearly rather than in quadrature with the other errors.

<sup>5</sup>We thank Geri Ganis for a recent update to this code.



### 3.4 Neutralino Relic Density

As already mentioned, we assume that the neutralino LSP constitutes essentially all the cold dark matter, for which we consider the allowed range to be [20]:

$$0.0855 < \Omega_\chi h^2 < 0.1189, \quad (11)$$

as mandated by WMAP and other observations.

As discussed in more detail in the Appendix, we have included in our calculation of the neutralino relic density, for the first time, all the processes for coannihilation between the three lightest neutralino states  $\chi_{1,2,3}$ , as well as with the lighter chargino  $\chi^\pm$  and with sleptons. The importance of  $\chi_1 - \chi_2 - \chi^\pm$  coannihilation has long been recognized within the context of the GUT-scale CMSSM [8,38]. Near the top-left boundary of the allowed region in the  $(m_{1/2}, m_0)$  plane, the lightest neutralino is Higgsino-like, near the bottom of the allowed region the lightest neutralino is bino-like, and the bino and Higgsino masses cross over along some intermediate contour. Near this cross-over line, and particularly where it intersects the left boundary of the allowed region in the  $(m_{1/2}, m_0)$  plane,  $\chi_1 - \chi_2 - \chi^\pm$  coannihilation is important in the GUT-scale CMSSM.

In the GUT-less CMSSM, as we show later, there are interesting regions of the  $(m_{1/2}, m_0)$  plane at small  $M_{in}$  where the  $\chi_3$  mass comes within  $\mathcal{O}(200)$  GeV of the  $\chi_2$  mass, and coannihilation processes involving the  $\chi_3$  can no longer be neglected. The reason for this, despite the relatively large  $\chi_3 - \chi_2$  mass difference, is that the couplings of the Higgsino-like  $\chi_3$  to relevant final states are significantly larger than the corresponding  $\chi_2$  couplings. Regions of the plane where  $\chi_2$  and  $\chi_3$  are degenerate are present at most values of  $M_{in}$ , though they typically occur when  $\chi_1$  is much lighter than the other neutralinos. For low  $M_{in}$ , however, there is in fact a near-degeneracy of all three of the lightest neutralinos as well as the lighter chargino. It is therefore necessary to include all coannihilations involving the three lightest neutralinos and the lighter chargino, as detailed in the Appendix.

In addition, we implement here various improvements to our previous treatment of the dark-matter density in regions where rapid annihilation via a direct-channel Higgs pole is important. Specifically, we have included further crossed-channel contributions to  $WW$ ,  $ZZ$  and less important processes.

## 4 Evolving Impact of the Cold Dark Matter Constraint

We now discuss the evolution of the dark matter constraint as the scale at which the soft supersymmetry breaking parameters are universal is lowered from the GUT scale. We assume  $m_t = 171.4$  GeV in this analysis. Deviation by a few GeV from this value would result in some change to the exact positions and shapes of the regions preferred by WMAP, but our results are quite general. We recall that, as usual in the CMSSM, the value of the Higgs mixing parameter  $\mu$  is fixed by the electroweak vacuum conditions, leaving its sign as a free parameter. Motivated by  $a_\mu$  and  $b \rightarrow s\gamma$ , we consider only  $\mu > 0$ , though a similar analysis could be carried out for negative  $\mu$ . In Sections 4.1 and 4.2 we discuss in detail the effects of lowering the universality scale for two values of the ratio of the Higgs vevs,  $\tan\beta = 10$

and  $\tan\beta = 50$ . We take  $A_0 = 0$  throughout Sections 4.1 and 4.2, and examine the impact of deviation from this assumption in Section 4.3. Related mirage-mediation models are discussed in Section 4.4.

## 4.1 Low $\tan\beta$

The evolution of the WMAP-preferred region in the  $(m_{1/2}, m_0)$  plane as the universality scale is lowered has been discussed previously in [15] for  $\tan\beta = 10$  and  $M_{in} \geq 10^{11.5}$  GeV. The WMAP-preferred regions found in this analysis, along with constraints from colliders, are shown in Figs. 2 and 3 for several values of  $M_{in}$ . To begin, we look first at the usual GUT-scale CMSSM scenario, shown in panel (a) of Fig. 2. One can see the  $\chi - \tilde{\tau}$  coannihilation region bordering the excluded stau LSP region for  $330 \lesssim m_{1/2} \lesssim 900$  GeV. Values of  $m_{1/2}$  below this range are excluded by the LEP Higgs constraint. Near  $m_{1/2} = 900$  GeV, the coannihilation strip dips down into the region where the  $\tilde{\tau}$  is the LSP. The focus point appears as a very thin strip tracking the border of the region excluded by the electroweak symmetry breaking condition at  $m_0 > 1500$  GeV. The LEP chargino bound also follows this boundary. The rapid-annihilation funnel is not present at  $\tan\beta = 10$  for  $M_{in}$  at the GUT scale, but will appear as the universality scale is lowered and also at larger  $\tan\beta$ .

As found in [15], there are already changes as the universality scale is lowered to  $M_{in} = 10^{14}$  GeV, shown in Panel (b) of Figure 2. The allowed focus-point region starts to separate from the LEP chargino bound, moving to larger  $m_{1/2}$ . Notice also that this strip does not join smoothly with the coannihilation strip, but instead is deflected due to rapid  $h$  annihilation near  $m_{1/2} \sim 150$  GeV. The region where the relic density falls in the WMAP range is thereby pushed inside the LEP chargino mass bound. However, this behavior occurs at low values of  $m_{1/2}$  which are excluded by the LEP Higgs bound as well.

For  $M_{in} = 10^{13}$  GeV, shown in panel (c) of Fig. 2, we notice that, as foreseen in Section 2, the regions excluded by the electroweak vacuum conditions and because the stau would be the LSP are encroaching further into the plane as  $M_{in}$  decreases, and the LEP Higgs bound is moving to larger  $m_{1/2}$ . We see in panel (c) of Fig. 2 that the allowed focus-point region also dips further down, away from the electroweak vacuum condition boundary, while the coannihilation strip moves up and farther away from the region where the stau is the LSP. In fact, the focus-point and coannihilation regions connect, forming an slender atoll extending to  $(m_{1/2}, m_0) \sim (2850, 2400)$  GeV (beyond the displayed region of the plane), inside which the relic density of neutralinos is too large. Another remarkable feature at this value of  $M_{in}$  is the appearance of the rapid-annihilation funnel, familiar in the GUT-scale CMSSM at large  $\tan\beta$ , but an unfamiliar feature for  $\tan\beta = 10$ . In the narrow space between the underside of the atoll and the thin WMAP-preferred strip lying approximately 100 – 200 GeV below it,  $2m_\chi \sim m_A$  and direct-channel annihilation processes are enhanced, causing the relic density to drop below the value determined by WMAP.

As the universality scale is further decreased to  $M_{in} = 10^{12.5}$  GeV, as shown in panel (d) of Fig. 2, the atoll formed by the conjunction of what had been the focus-point and coannihilation strips has shrunk, so that it lies entirely within the range of  $(m_{1/2}, m_0)$  shown

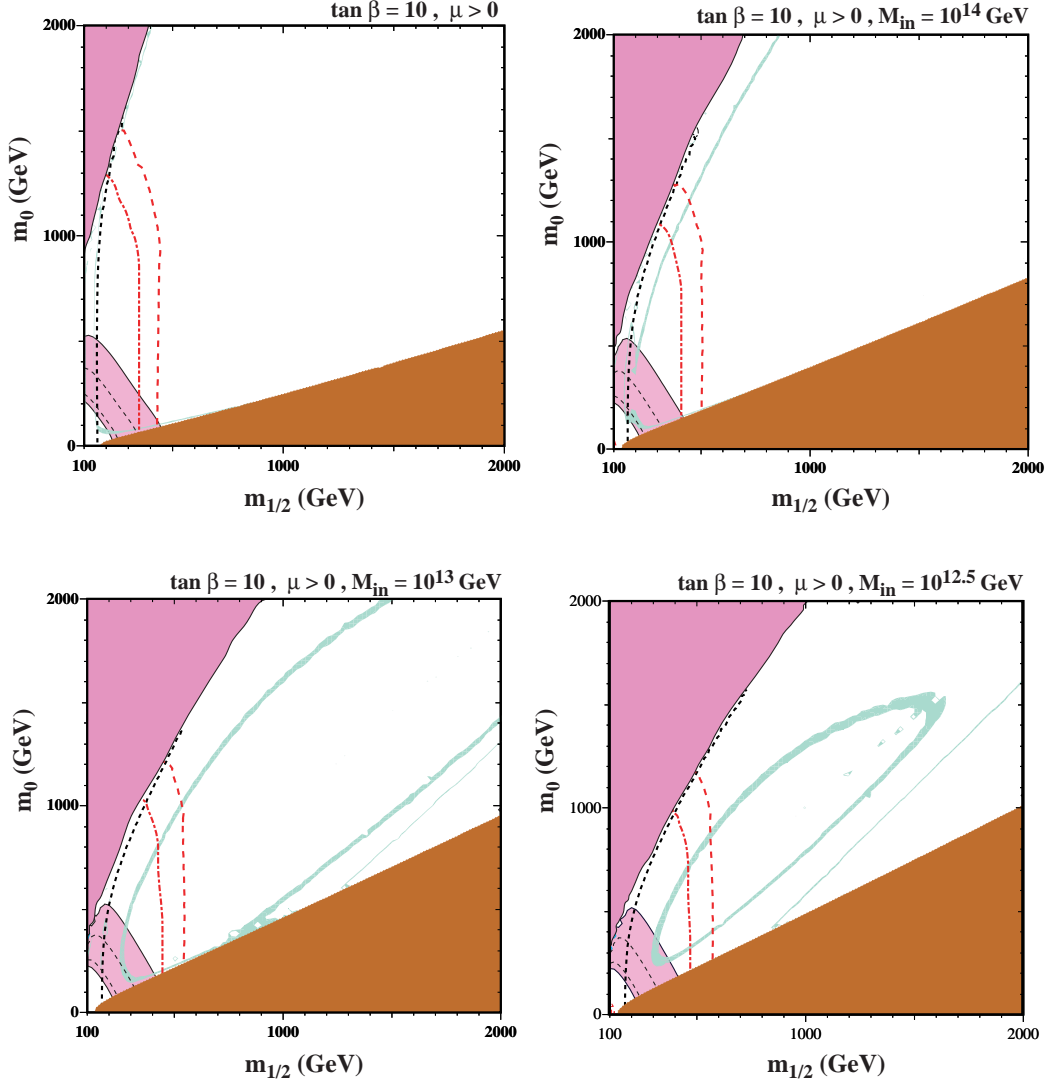


Figure 2: *Examples of  $(m_{1/2}, m_0)$  planes with  $\tan \beta = 10$  and  $A_0 = 0$  but with different values of  $M_{in}$ . (a) The CMSSM case with  $M_{in} = M_{GUT} \sim 2 \times 10^{16} \text{ GeV}$ , (b)  $M_{in} = 10^{14} \text{ GeV}$ , (c)  $M_{in} = 10^{13} \text{ GeV}$  and (d)  $M_{in} = 10^{12.5} \text{ GeV}$ . In each panel, we show contours representing the LEP lower limits on the chargino mass (black dashed line), a Higgs mass of 114 GeV (red dashed), and the more exact (and relaxed) Higgs bound (red dot-dashed). We also show the region ruled out because the LSP would be charged (dark red shading), and that excluded by the electroweak vacuum condition (dark pink shading). The region favoured by the WMAP range  $\Omega_{CDM} h^2 = 0.1045^{+0.0072}_{-0.0095}$  has light turquoise shading, and the region suggested by  $g_\mu - 2$  at 2- $\sigma$  has medium (pink) shading, with the 1- $\sigma$  contours shown as black dashed lines.*

in panel (d)<sup>6</sup>. We now see clearly two distinct regions of the plane excluded due to an excess relic density of neutralinos; the area enclosed by the atoll and the slice between the lower funnel wall and the boundary of the already-excluded  $\tilde{\tau}$ -LSP region.

The four panels of Figure 3 show the consequences of lowering the universality scale even further, down as far as  $M_{in} = 10^9$  GeV. In panel (a) for  $M_{in} = 10^{12}$  GeV, the focus-point and coannihilation regions are fully combined and the atoll has mostly filled in to become a small island of acceptable relic density. To the right of this island is a strip that is provided by the lower funnel wall. The strip curves slightly as  $m_{1/2}$  increases then takes a sharp plunge back down towards the boundary of the region where the stau is the LSP, a feature associated with the  $\chi\chi \rightarrow h + A$  threshold. Reduction in the universality scale from this point results in the lower funnel wall being pushed down into the excluded  $\tilde{\tau}$  LSP region and total evaporation of the island.

As the universality scale decreases further in panels (b), (c) and (d) for  $M_{in} = 10^{11}$  GeV,  $10^{10}$  GeV and  $10^9$  GeV, respectively, we see only a small residual turquoise region at large  $m_{1/2}$  where the relic density is within the WMAP limits. At all other points in the visible part of the  $(m_{1/2}, m_0)$  plane the relic density of neutralinos is too low to provide fully the cold dark matter density preferred by WMAP *et al.* Of course, these SUSY models would not be excluded if there is another source of cold dark matter in the universe.

In these last four panels, we notice that the boundary of the region where the stau is the LSP is retreating back down to smaller  $m_0$ , as expected from the discussion of evolution with  $M_{in}$  of the masses of the stau and the lightest neutralino given in Section 2.

## 4.2 High $\tan\beta$

The situation at larger  $\tan\beta$  looks somewhat different at first glance. In the GUT-scale CMSSM case, shown in panel (a) of Fig. 4, we see the familiar regions excluded because of a  $\tilde{\tau}$  LSP and the electroweak vacuum condition. The LEP Higgs and chargino mass bounds have impacts similar to those in the low- $\tan\beta$  scenario. The region excluded by  $b \rightarrow s\gamma$  decay has grown substantially, and a new region excluded by the limit  $BR(B_s \rightarrow \mu^+ \mu^-) > 1 \times 10^{-7}$  appears at low  $(m_{1/2}, m_0)$ , which is, however, already excluded by other constraints. As for the relic density, the focus-point region is visible as a strip tracking the electroweak vacuum condition for  $m_0 > 1050$  GeV, whereas the region preferred by WMAP is excluded by the LEP Higgs constraint at smaller  $m_0$ . Along the excluded  $\tilde{\tau}$  LSP boundary, we see that the familiar coannihilation strip is truncated at low  $m_{1/2}$  by the Higgs and chargino mass constraints, and also by  $B_s \rightarrow \mu^+ \mu^-$ . Following this strip to larger  $m_{1/2}$ , there is the familiar rapid-annihilation funnel, where  $2m_{\chi_1} \sim m_A$  and the relic density is kept in the range preferred by WMAP by annihilations through the direct-channel  $A$  and  $H$  poles, which lifts away from the excluded region.

However, at large  $\tan\beta$ , even small changes in the universality scale make a dramatic difference in the appearance of the regions preferred by WMAP. At  $M_{in} = 10^{15.5}$  GeV, as

---

<sup>6</sup>We note a string of bubbles intruding into the atoll, which are due to a significant enhancement of  $t$ -channel exchange in  $\chi_2\chi_2 \rightarrow h + (H, A)$ . The analysis of these possible regions of small relic density would require a complete treatment of poles, including finite-width effects, which we do not attempt here.

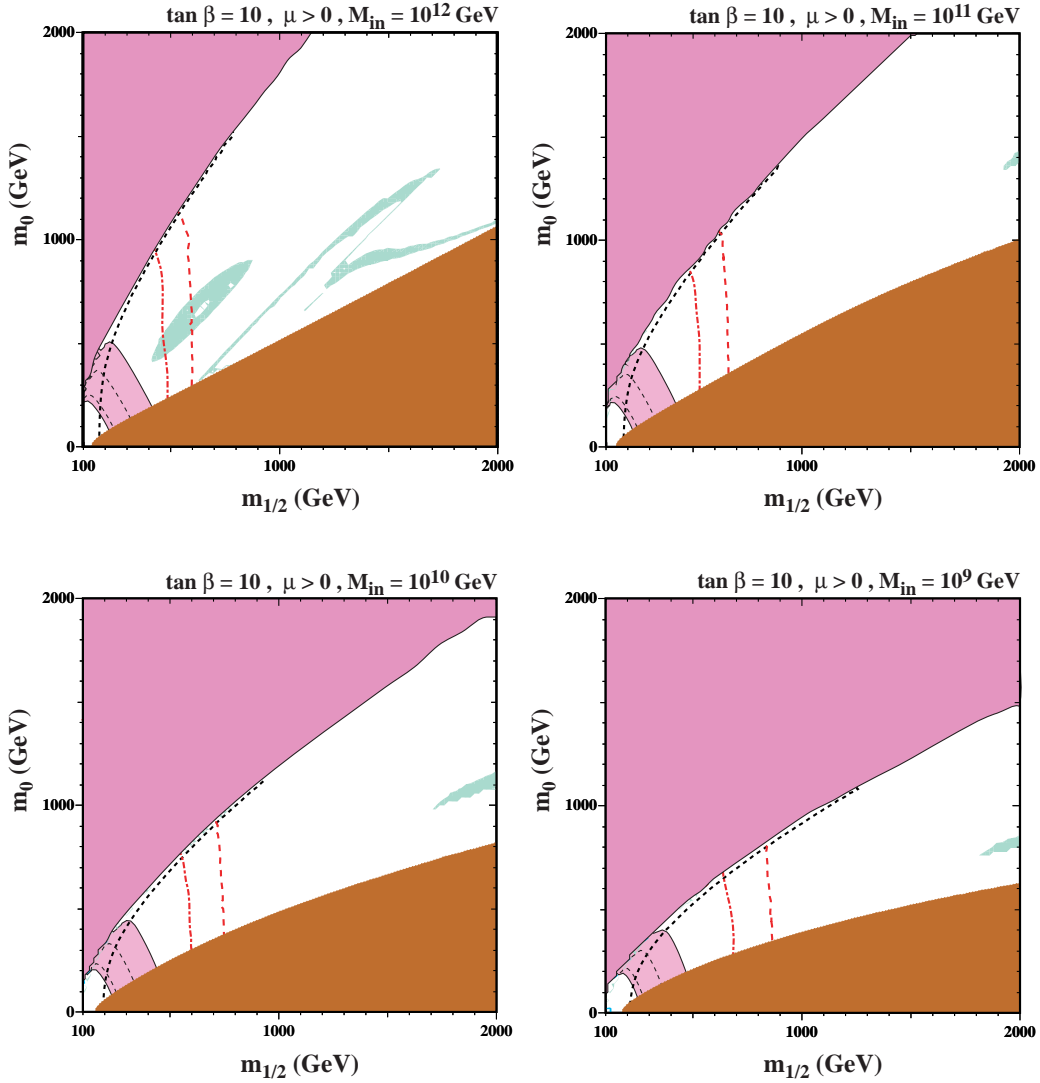


Figure 3: *Further examples of  $(m_{1/2}, m_0)$  planes with  $\tan\beta = 10$  and  $A_0 = 0$  but with different values of  $M_{in}$ : (a)  $M_{in} = 10^{12}$  GeV, (b)  $M_{in} = 10^{11}$  GeV, (c)  $M_{in} = 10^{10}$  GeV and (d)  $M_{in} = 10^9$  GeV. The various contours and shadings are the same as for Fig. 2.*

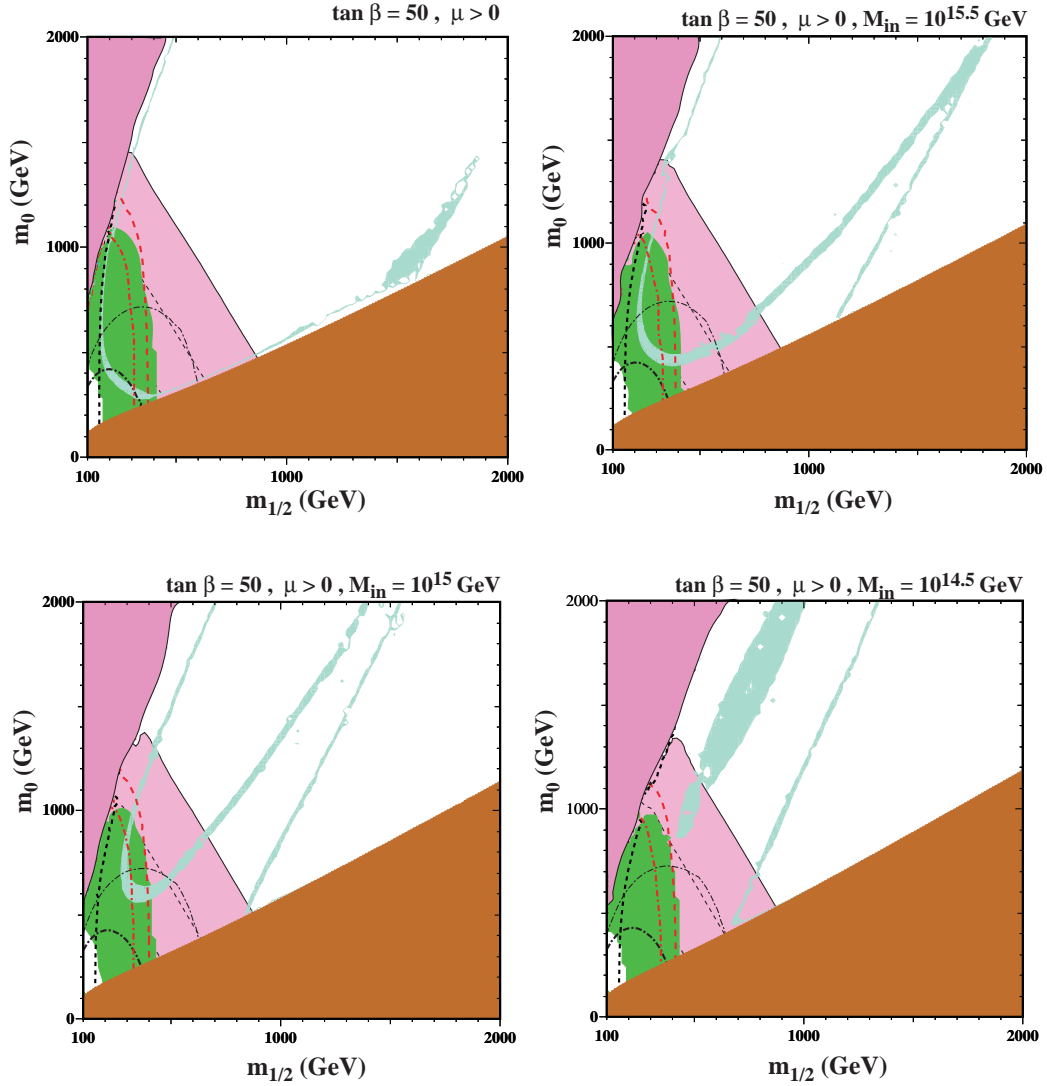


Figure 4: *Examples of  $(m_{1/2}, m_0)$  planes with  $\tan \beta = 50$  and  $A_0 = 0$  but with different values of  $M_{in}$ . (a) The CMSSM case with  $M_{in} = M_{GUT} \sim 2 \times 10^{16}$  GeV, (b)  $M_{in} = 10^{15.5}$  GeV, (c)  $M_{in} = 10^{15}$  GeV and (d)  $M_{in} = 10^{14.5}$  GeV. In addition to the constraints enumerated in the caption to Fig. 2, we also show the regions ruled out by  $b \rightarrow s\gamma$  decay [31, 33, 34] (medium green shading) and black dot-dashed contours representing the current CDF limit on the rate of  $B_s \rightarrow \mu^+ \mu^-$  ( $1 \times 10^{-7}$ ) and a projected sensitivity of the Tevatron and the LHC experiments ( $2 \times 10^{-8}$ ).*

seen in panel (b) of Fig. 4, the coannihilation strip and rapid-annihilation funnel have joined to create a large funnel region that extends to  $(m_{1/2}, m_0) \sim (1850, 2000)$  GeV. Inside the funnel boundary, effects such as rapid annihilation near the  $A$  pole and the coannihilations of neutralinos with light sleptons combine to cause the relic density to fall below the range preferred by WMAP. In this region of low relic density, the lightest neutralino is bino-like, and the dominant annihilations are into  $b\bar{b}$  and  $\tau\bar{\tau}$  pairs. As in the GUT-scale universality scenario, the focus-point region is cut off at  $m_0 \sim 950$  GeV by the LEP Higgs constraint. At this universality scale, values of  $m_{1/2} > 600$  GeV are compatible also with  $m_0 > 2000$  GeV, beyond the displayed region of the  $(m_{1/2}, m_0)$  plane.

As the universality scale is further reduced to  $M_{in} = 10^{15}$  GeV, we see in panel (c) of Fig. 4 that the funnel is elongated further and opens wider at the top, while simultaneously the focus-point region falls significantly below the zone excluded by the electroweak vacuum conditions. In addition, the bulk region, where the upper funnel wall connects to the focus point, has now shifted to larger  $m_{1/2}$ , so that it lies mostly outside the LEP Higgs bound. As in the other panels of this figure, the regions currently excluded by  $B_s \rightarrow \mu^+ \mu^-$  are also excluded by  $b \rightarrow s\gamma$ . We note that, as  $M_{in}$  decreases, the bulk and focus-point regions are moving to larger  $m_{1/2}$  more rapidly than the LEP Higgs constraint, resulting in a larger WMAP-preferred region at small  $m_{1/2}$  and  $m_0$ . At the same time, however, the upper funnel wall is moving to smaller  $m_{1/2}$ , causing the region between the focus point and the upper funnel wall (where the relic density is too large) to shrink.

To illustrate how the relic density changes with  $m_{1/2}$  and its sensitivity to various interactions, we follow the evolution of the relic density for  $M_{in} = 10^{15}$  GeV at a fixed value of  $m_0 = 1000$  GeV. At very low  $m_{1/2} < 240$  GeV, the electroweak symmetry breaking conditions would impose an unphysical solution for the weak scale value of the Higgs mass parameter, so this region of the plane is excluded, as discussed in Section 2. Near the boundary of the excluded region,  $\mu \lesssim m_{1/2}$ , so the LSP has a strong higgsino component and annihilations to light fermions keep the relic density low. As one moves to larger  $m_{1/2}$ , the bino component increases, causing the relic density to increase accordingly, though it remains below the WMAP-preferred range. At  $m_{1/2} = 244$  GeV, the  $\chi\chi \rightarrow W^+W^-$  threshold is reached and the relic density decreases dramatically, only to start rising again once the threshold is passed. By  $m_{1/2} = 280$  GeV, the LSP has become bino-like, though it still has substantial higgsino components.

Near  $m_{1/2} = 325$  GeV, the relic density has risen to the range preferred by the WMAP measurements, and continues to increase until it exceeds the WMAP range. The thinness of the WMAP strip indicates the rate at which the relic density is increasing, reaching its peak value near  $m_{1/2} = 500$  GeV. As  $m_{1/2}$  increases further, one approaches the broad  $(H, A)$  pole region, where s-channel annihilations cause the relic density to decrease dramatically. Thus, the upper funnel wall appears near  $m_{1/2} = 750$  GeV, and the relic density then continues to plummet until  $m_\chi$  becomes large enough that the pole has been passed, at which point the relic density again increases until it falls within the WMAP range for a third time near  $m_{1/2} = 1080$  GeV, forming the lower wall of the funnel region. As  $m_{1/2}$  increases further, the relic density of neutralinos becomes too large to be compatible with the WMAP measurement. Near the border of the  $\tilde{\tau}$  LSP region, the relic density decreases

due to enhanced  $\chi - \tilde{\tau}$  coannihilations, however the effect is not sufficient to bring it down to the WMAP range. All values of  $m_{1/2}$  to the right of the lower funnel wall are excluded by the large relic density of neutralinos.

When  $M_{in} = 10^{14.5}$  GeV, the focus-point region and upper funnel wall merge fully to form an island of acceptable relic density, extending from  $(m_{1/2}, m_0) \sim (400, 850)$  GeV to large  $m_0$ , parallel to the lower funnel wall, and with a width of  $\sim 200$  GeV at its broadest point.

In Fig. 5, as in the  $\tan\beta = 10$  scenario, we see the electroweak vacuum condition creep further down into the plane, as  $M_{in}$  is further reduced. The  $\tilde{\tau}$  LSP region also retreats to smaller  $m_0$ , because of the  $M_{in}$  dependences of the sparticle masses discussed in Section 2. When the universality scale is  $M_{in} = 10^{14}$  GeV, as seen in panel (a) of Fig. 5, this island has submerged and disappeared as enhanced annihilations to  $b\bar{b}$  and  $\tau\bar{\tau}$  dominate even for  $2m_{\chi_1} < m_A$ . Coannihilations of  $\chi_0$  with  $\chi_i$ , where  $\chi_i$  denote the second- and third-lightest neutralinos, also play a significant role in the smallness of the relic density in this region. The only values of  $m_{1/2}$  and  $m_0$  for which the relic density of neutralinos is in agreement with the WMAP measurement are in the thin strip that had been the lower funnel wall, and a narrow coannihilation strip adjacent to the  $\tilde{\tau}$  LSP region. To the left of the residual funnel strip, the relic density is below the WMAP value, whereas this value is exceeded in the ‘vee’ between the funnel and coannihilation strips at large  $m_{1/2}$ . At  $M_{in} = 10^{14}$  GeV, all values of  $m_{1/2} > 1230$  GeV are excluded for  $m_0 < 2000$  GeV.

In panel (b) for  $M_{in} = 10^{13}$  GeV, what is left of the lower funnel wall is also beginning to curve down. This is the same general behavior we observed in the  $\tan\beta = 10$  case. As the universality scale is slightly reduced, to  $M_{in} = 10^{12.5}$  GeV (not shown), this strip bends down into the  $\tilde{\tau}$  LSP region at  $(m_{1/2}, m_0) \sim (2000, 1450)$  GeV. For  $M_{in} = 10^{12}$  GeV, as seen in panel (c) of Fig. 5, there remains only a small ellipse where the relic density falls in the region preferred by WMAP. The rest of the plane not excluded by the electroweak vacuum condition or the charged LSP constraint has a relic density of neutralinos smaller than that required by WMAP<sup>7</sup>. This last remaining WMAP island evaporates as the universality scale is decreased to  $10^{11}$  GeV, as seen in panel (d) of Fig. 5, at which point the entire plane is disfavoured, in the sense that some additional source of cold dark matter would be required.

### 4.3 Non-Zero $A_0$

To this point, we have considered all trilinear soft supersymmetry-breaking parameters to be zero at the unification scale,  $A_0 = 0$ . Here we limit ourselves to a brief discussion of  $A_0 \neq 0$  as preparation for the discussion of mirage-mediation models in the next Section.

If  $A_0 > 0$ , the RGEs generate correspondingly larger trilinear couplings at the weak scale. In addition, since the large loop corrections to  $\mu$  depend on the values of the trilinear couplings, there is also an increase in  $\mu$ . We therefore expect, based on the discussion in Section 2, that the region excluded by the electroweak vacuum condition decreases with increasing  $A_0$ . Other striking differences in the  $(m_{1/2}, m_0)$  plane are in the constraints on the

---

<sup>7</sup>We stress again that such regions are not excluded, provided there is another source of cold dark matter in the Universe.



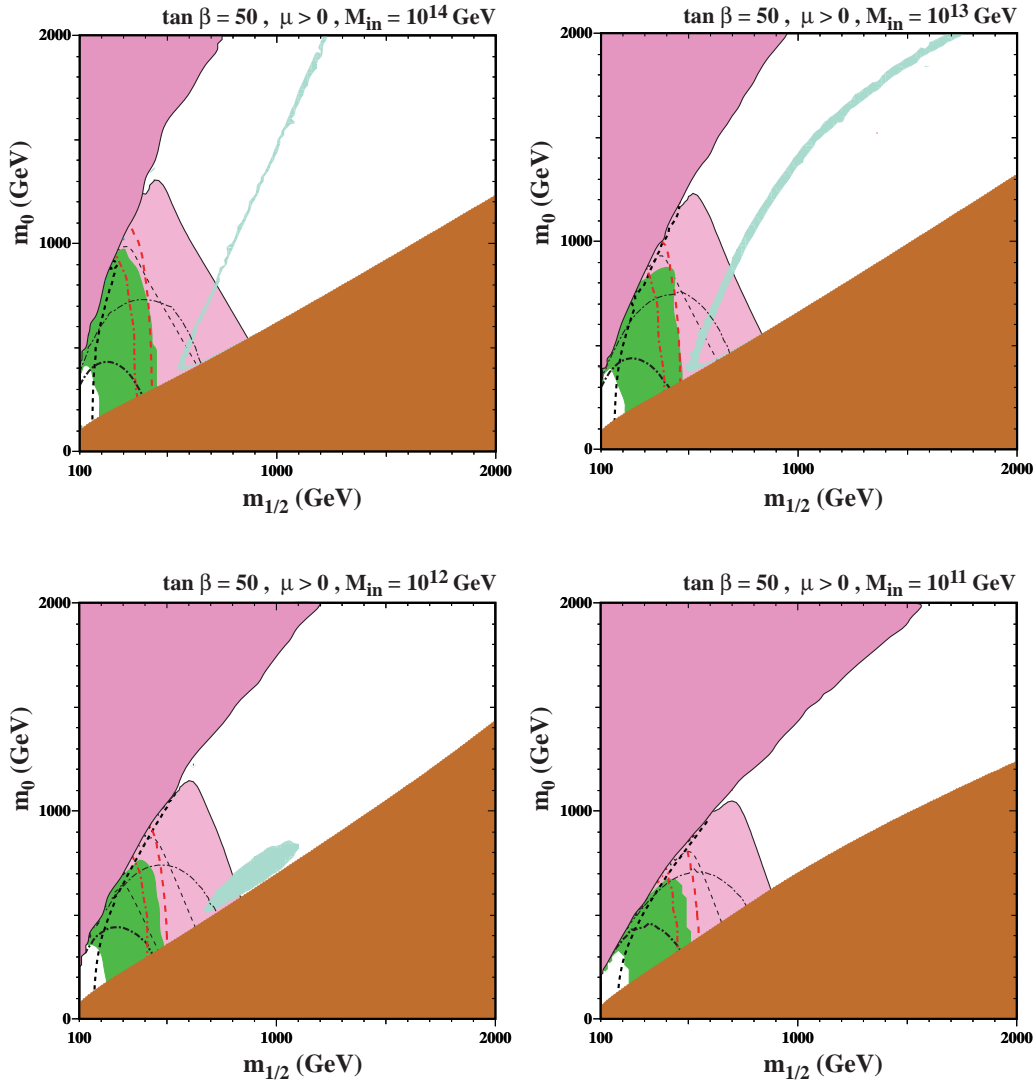


Figure 5: *Examples of  $(m_{1/2}, m_0)$  planes with  $\tan \beta = 50$  and  $A_0 = 0$  but with different values of  $M_{in}$ . (a)  $M_{in} = 10^{14}$  GeV, (b)  $M_{in} = 10^{13}$  GeV, (c)  $M_{in} = 10^{12}$  GeV and (d)  $M_{in} = 10^{11}$  GeV. The various contours and shadings are the same as for Fig. 4.*

Higgs mass and the  $b \rightarrow s\gamma$  rate. While the LEP Higgs constraint is dramatically relaxed for larger  $A_0$ , the region excluded by  $b \rightarrow s\gamma$  increases in size, becoming the dominant constraint for low  $m_{1/2}$ . Furthermore, since the off-diagonal elements of the squark mass matrix contain terms proportional to the negative of the trilinear couplings, when  $A_0$  is large these off-diagonal contributions can become large enough to drive the lightest stop quark mass below the LEP bound. As a result, we see a new excluded region emerge at low  $m_{1/2}$  and  $m_0$ , where the lighter stop has  $m_{\tilde{t}} < 220$  GeV [39].

For  $A_0$  negative, the changes to the constraints discussed above are quite predictable. In this case, the RGE's generate correspondingly smaller weak scale trilinear couplings, resulting in a universally smaller  $\mu$ . The LSP is then more more Higgsino-like over the whole plane. The LEP Higgs bound is strengthened, and the  $b \rightarrow s\gamma$  rate becomes an insignificant constraint.

The regions of the plane where the relic density of neutralinos is in the measured range also change shape for  $A_0 \neq 0$ . In general, these changes can be ascribed to one of two effects. First, in addition to the  $\tilde{\tau}\chi$  coannihilation strip, there may be an additional  $\tilde{t}\chi$  coannihilation strip, where the lighter stop is degenerate with the neutralino LSP. This feature is common in scenarios with large  $A_0$  and both the  $\tilde{t}\chi$  coannihilation strip and the excluded light stop region move further into the plane as  $A_0$  is increased. Secondly, we recall that the composition of the LSP depends on the ratio of  $\mu$  to  $M_1$ , the LSP being bino-like when  $M_1$  is small compared to  $\mu$  and Higgsino-like if  $\mu$  is small compared to  $M_1$ , as shown in panel (d) of Figure 1. Since  $\mu$  is enhanced everywhere in the plane when  $A_0 > 0$ , we expect the LSP to be generically more bino-like than when  $A_0 = 0$ . Similarly, we expect the LSP to be generically more Higgsino-like when  $A_0 < 0$ . For  $M_{in} \approx M_{GUT}$  (not pictured), the LSP is strongly bino-like over most of the plane, so the main effects of  $A_0 \neq 0$  are the above-mentioned modifications in the constraints, and the appearance of the  $\tilde{t}\chi$  coannihilation strip for large positive  $A_0$ .

For lower unification scales, however, the LSP has more substantial Higgsino components, becoming Higgsino-dominated over much of the plane for very low  $M_{in}$ . Larger  $\mu$  means that the LSP will remain bino-like even for larger values of  $M_1$ , so in scenarios with  $A_0 > 0$  the LSP is more bino-like and the heavier neutralinos with large Higgsino components are even heavier than when  $A_0 = 0$ . These differences are clear at low  $M_{in}$ , when the LSP is becoming Higgsino-like over much of the plane when  $A_0 = 0$  but is still bino-like when  $A_0$  has a sufficiently large positive value. In panel (a) of Fig. 6, we show the  $(m_{1/2}, m_0)$  plane for  $\tan\beta = 10$ ,  $M_{in} = 10^{12}$  GeV, and  $A_0 = 1000$  GeV. We note the similarity to panel (d) of Fig. 2, where  $M_{in} = 10^{12.5}$ . When  $A_0 > 0$ , smaller values of  $\mu$  appear only at values of  $M_{in}$  that are lower than in the  $A_0 = 0$  cases previously discussed. In the same way, the  $A_0 < 0$  case tends to mimic the effect of larger  $M_{in}$ . With respect to the relic density of neutralinos, there is some degeneracy in the parameters  $M_{in}$  and  $A_0$  for regions of the  $(m_{1/2}, m_0)$  plane far from the  $\tilde{t}\chi$  coannihilation strip.

We note that  $A_0 \propto M$ , where  $M = m_{1/2}$  or  $m_0$ , is also a viable possibility, the consequences of which, in light of the above discussion, are easily understood. In these cases, for small  $M$ , the plane will be similar to the  $A_0 = 0$  case, while at larger  $M$ , the changes described above will be increasingly evident. A complete discussion of  $A_0 \neq 0$  or non-universal

$A_0$  is beyond the scope of this study.

## 4.4 Mirage-Mediation Models

Models in which supersymmetry breaking occurs through some combination of modulus and anomaly mediation are among those characterized by the apparent unification of gaugino and scalar mass parameters at an intermediate scale. As a result, these models have been termed mirage-mediation models [17]<sup>8</sup>, and the unification scale, the mirage messenger scale, is estimated to be  $\sim 10^{10} - 10^{12}$  GeV. One distinctive feature of these scenarios is that the gaugino and scalar masses run both above and below the unification scale. Here, we discuss briefly the effect on our results of the additional running of the masses above the unification scale.

The use of the RGEs to run the masses down from the input scale to the weak scale is unchanged, and the procedure for calculating the weak-scale observables is unchanged, regardless whether the soft supersymmetry-breaking mass parameters run above the unification scale. The chief difference derives from the fact that the value of  $\mu$  is fixed by the electroweak vacuum conditions, which include a large dependence on the trilinear couplings as discussed in the previous section. When the trilinear couplings run from the GUT scale, becoming larger as the energy scale decreases, they attain larger weak-scale values than would be possible with running only below  $M_{in}$ . Therefore, in mirage-mediation models  $\mu$  receives a large contribution from the exceptionally large values of the trilinear couplings at the weak scale. The resulting picture for mirage-mediation models is similar to what one would expect from the GUT-less cases with  $A_0 \neq 0$ , as discussed above. It should be noted that the trilinear couplings in mirage-mediation scenarios, as well as the other soft SUSY-breaking parameters, are specified at the GUT scale based on the particular mixture of modulus and anomaly mediation. The soft SUSY-breaking parameters are taken to be proportional to each other, with constants of proportionality determined by the modular weights and other considerations [17]. For simplicity, we consider only  $A_0 = 0$  at the GUT scale.

In panel (b) of Fig. 6 we show the  $(m_{1/2}, m_0)$  plane with running of the gaugino and scalar masses both above and below the unification scale for  $M_{in} = 10^{11}$  GeV and  $\tan\beta = 10$ . There is a broad region of acceptable relic density lying just above the excluded  $\tilde{\tau}$  LSP region. For comparison, in the standard GUT-less case for  $M_{in} = 10^{11}$  GeV shown in panel (b) of Fig. 3, as discussed already in Section 4.1, the relic density of neutralinos is below the WMAP  $2\text{-}\sigma$  range throughout the plane, except in the small island just barely in view at  $m_{1/2} = 2000$  GeV.

There are a few important differences worthy of note. First, the value of  $\mu$  all over the plane is universally larger in the mirage-mediation scenario than in the cases discussed previously in this paper, which is attributed to the running of  $A_0$  from the GUT scale rather than  $M_{in}$ . As a result, we expect the boundary of the region excluded by the electroweak vacuum conditions to be pushed back up into the upper left corner of the plane, as is seen. A second important consequence concerns the composition of the LSP. Recalling that the LSP

---

<sup>8</sup>Such models are motivated, e.g., by the KKLT framework [19].

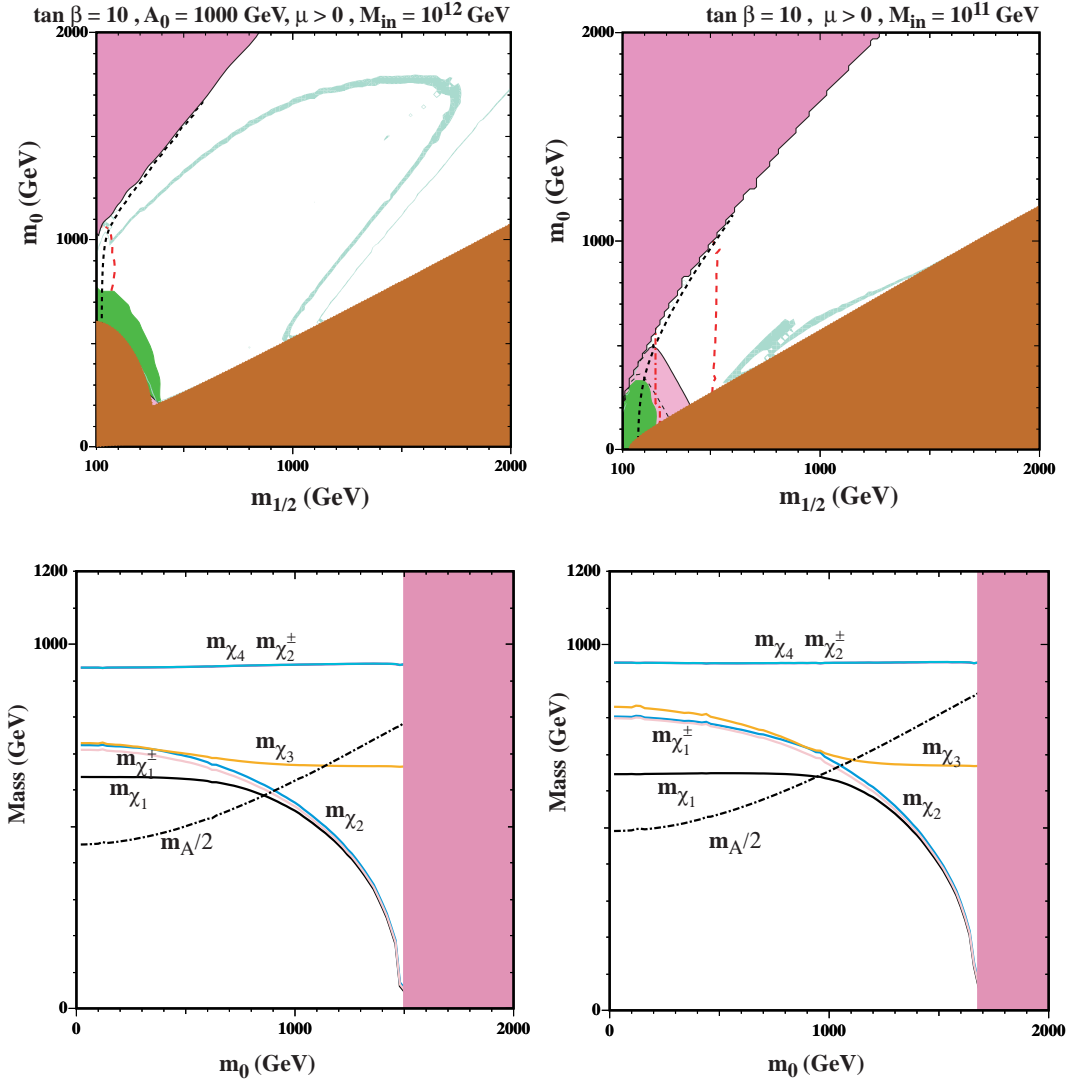


Figure 6: Panel (a) shows the  $(m_{1/2}, m_0)$  plane for the GUT-less case with  $\tan\beta = 10$ ,  $M_{in} = 10^{12}$  GeV, and  $A_0 = 1000$  GeV. Panel (b) displays a scenario similar to that found in mirage-mediation models, where the soft supersymmetry-breaking parameters are universal at  $M_{in} = 10^{11}$  GeV, but run both above and below this scale. The weak-scale values of the neutralino and chargino masses, as well as the pseudoscalar Higgs mass and  $\mu$ , are shown in panel (c) for the usual GUT-less case with  $A_0 = 0$  and  $M_{in} = 10^{11}$  as shown in panel (b) of Fig. 3. Panel (d) shows the same information as panel (c) for the mirage-mediation case.

is bino-like as long as  $M_1$  is much smaller than  $\mu$ . The fact that  $\mu$  is larger in the mirage-mediation case implies that the cross-over when  $M_1 \approx \mu$  takes place at a lower unification scale than was found in panel (d) of Fig. 1. In fact, the LSP is bino-like over most of the plane in the mirage-mediation case shown in panel (b) of Fig. 6, whereas it has large Higgsino components for much of the standard GUT-less plane for the same value of  $M_{in}$ . Similarly, the heavier neutralinos, which have large Higgsino components, are even heavier due to the enhancement in  $\mu$  in mirage-mediation models. This effect can be seen clearly by comparing panels (c) and (d) of Fig. 6.

## 5 Neutralino-Nucleon Cross Sections

Direct searches for dark matter particles such as the Cryogenic Dark Matter Search (CDMS) [40] and other experiments look for evidence of weakly-interacting massive particles (WIMPs) through scattering on nuclei. In this section, we present the predictions for neutralino-nucleon scattering cross sections in the scenarios discussed above [41] - [48].

The low-energy effective interaction Lagrangian for elastic  $\chi$ -nucleon scattering can be written as

$$L = \alpha_{2i} \bar{\chi} \gamma^\mu \gamma^5 \chi \bar{q}_i \gamma_\mu \gamma^5 q_i + \alpha_{3i} \bar{\chi} \chi \bar{q}_i q_i, \quad (12)$$

where terms that make velocity-dependent contributions to the cross section have been neglected, and the constants  $\alpha_{2i}$  and  $\alpha_{3i}$  are defined as in Ref. [43]. In computing the scalar cross section, we have assumed the pi-nucleon  $\Sigma$  term to be 64 MeV (see [49] for the sensitivity of the elastic cross section to this assumption). Summation over the quark generations is implied, with up- and down-type quarks labeled by the subscript  $i$ . The cross section can be broken into a spin-dependent part arising from the term proportional to  $\alpha_{2i}$  and a spin-independent (scalar) part from the term proportional to  $\alpha_{3i}$ . The spin-dependent cross section is, in general, larger than the scalar cross section. However, since the whole nucleus participates coherently in spin-independent interactions, it is primarily the scalar cross section that is probed by current direct-detection experiments. On the other hand, the spin-dependent scattering cross section on the proton plays an important role in the capture and annihilation rates inside the Sun.

Figs. 7 and 8 show scatter plots of the spin-dependent and scalar cross sections for elastic  $\chi$ -nucleon scattering. We plot the cross sections as functions of the neutralino mass for points in the  $(m_{1/2}, m_0)$  plane where the relic density of neutralinos is less than the 2- $\sigma$  upper limit from WMAP (as first examined in Ref. [50]) with the assumption of universality at the GUT scale relaxed. For the cases where the relic density is smaller than the central WMAP value, indicating that there must be another source of astrophysical cold dark matter, we plot the cross section scaled by the ratio of the relic density of neutralinos to the central density of cold dark matter inferred from WMAP measurements of the CMB. These results can be compared with the direct-detection limits available from CDMS and other experiments. In each figure, we also show the CDMS II limit for the scalar part of the neutralino-nucleon cross section [51]. Current limits on the spin-dependent cross section are  $\sigma_{\chi n} \lesssim 10^{-1}$  pb [52], which lies outside the range we have plotted in Figures 7 and 8. We require that the

lightest neutralino be the LSP and that electroweak symmetry be broken, as usual. The LEP constraint on the chargino mass has been applied, as discussed in Section 3.1. Different colors in Figures 7 and 8 indicate whether the point lies within the region excluded by  $b \rightarrow s\gamma$  decay or the LEP Higgs mass constraint. The dark blue (striped) regions are the spin-dependent (scalar) cross sections that pass all these constraints. Lighter (green) regions in each panel fail the relaxed LEP Higgs constraint. At large  $\tan\beta$ , when the constraint on the rate of  $b \rightarrow s\gamma$  becomes dominant, we show in red the regions that fail this constraint but pass all others.

The results for  $\tan\beta = 10$  are shown in Figure 7 for four different values of  $M_{in}$ . The spin-dependent cross sections lie above the scalar cross sections in each of the four panels. As  $M_{in}$  is lowered, the number of points increases dramatically and they spread to larger  $m_\chi$ . This is due to the fact that the relic density over all of the  $(m_{1/2}, m_0)$  plane decreases as  $M_{in}$  decreases, so that less and less of the plane is excluded by having an excess relic density<sup>9</sup>.

We turn our attention first to the usual GUT-scale CMSSM, in which the relic density is too large over most of the  $(m_{1/2}, m_0)$  plane. Within the allowed regions for each of the spin-dependent and scalar cross sections, we can identify two separate behaviours. First, there is a region stretching out to  $m_\chi \sim 350$  GeV where the cross section may vary over as much as an order of magnitude for some values of  $m_\chi$ . This feature corresponds to the coannihilation strip, which is shown in Figure 2 to dip into the  $\tilde{\tau}$ -LSP excluded region near  $m_{1/2} = 900$  GeV. The variation in the cross section in this coannihilation strip region at low  $m_\chi$  in panel (a) is due to the separation of the coannihilation strip from the boundary of the  $\tilde{\tau}$ -LSP region at low  $m_{1/2}$ . The cross sections for points lying between the coannihilation strip and the forbidden  $\tilde{\tau}$ -LSP region, where the relic density of neutralinos is too low, are scaled down to reflect the fact that in these cases the neutralinos can provide only a small fraction of the cold dark matter in the Universe.

The second region lies within  $80 \text{ GeV} < m_\chi < 170 \text{ GeV}$ . In the case of the spin-dependent cross section, the cross sections in this region are clearly separated from those due to the coannihilation strip. This second region of acceptable cross sections comes from the focus-point region which, for  $M_{in} = M_{GUT}$ , occurs at large  $m_0$  and small  $m_{1/2}$ . It should be noted that, if we were to consider values of  $m_0 > 2000$  GeV, the focus-point region would extend to larger  $(m_{1/2}, m_0)$ , so analogous focus-point cross sections would extend also to larger  $m_\chi$ . In the focus-point region, the fact that the lightest neutralino acquires substantial Higgsino components leads to an enhancement in the spin-dependent cross section due to  $Z$  exchange. Simultaneously, the scalar cross section becomes dominated by neutral Higgs exchange as the neutralino becomes Higgsino-like.

Panels (b), (c), and (d) show the neutralino-nucleon cross sections as functions of the neutralino mass for  $M_{in} = 10^{14}$ ,  $10^{12}$ , and  $10^{10}$  GeV, respectively. The changes in the cross sections as  $M_{in}$  is lowered may be understood by referring to the corresponding  $(m_{1/2}, m_0)$  planes from Figures 2 and 3. When  $M_{in} = 10^{14}$  GeV, the focus-point region becomes more prominent, separating from the boundary of the region excluded by the electroweak vacuum

---

<sup>9</sup>In fact, for  $M_{in} = 10^{10}$  GeV as shown in Panel (d), the constraint on the relic density does not exclude any points, but serves only as a scale factor for the cross sections.

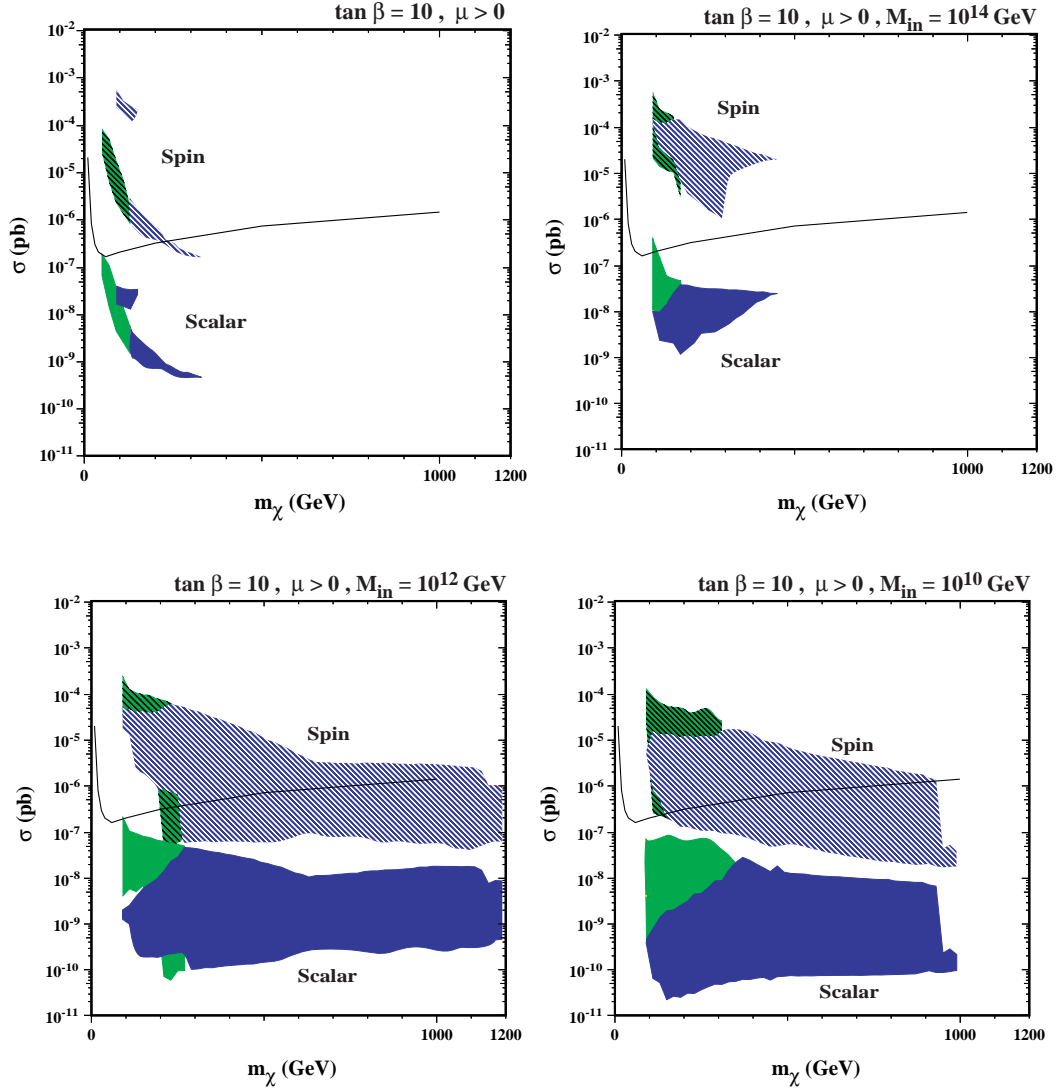


Figure 7: Neutralino-nucleon cross sections as functions of the neutralino mass for  $\tan\beta = 10$  and  $A_0 = 0$  but with different values of  $M_{in}$ . (a)  $M_{in} = M_{GUT} \approx 2 \times 10^{16}$  GeV, (b)  $M_{in} = 10^{14}$  GeV, (c)  $M_{in} = 10^{12}$  GeV and (d)  $M_{in} = 10^{10}$  GeV.

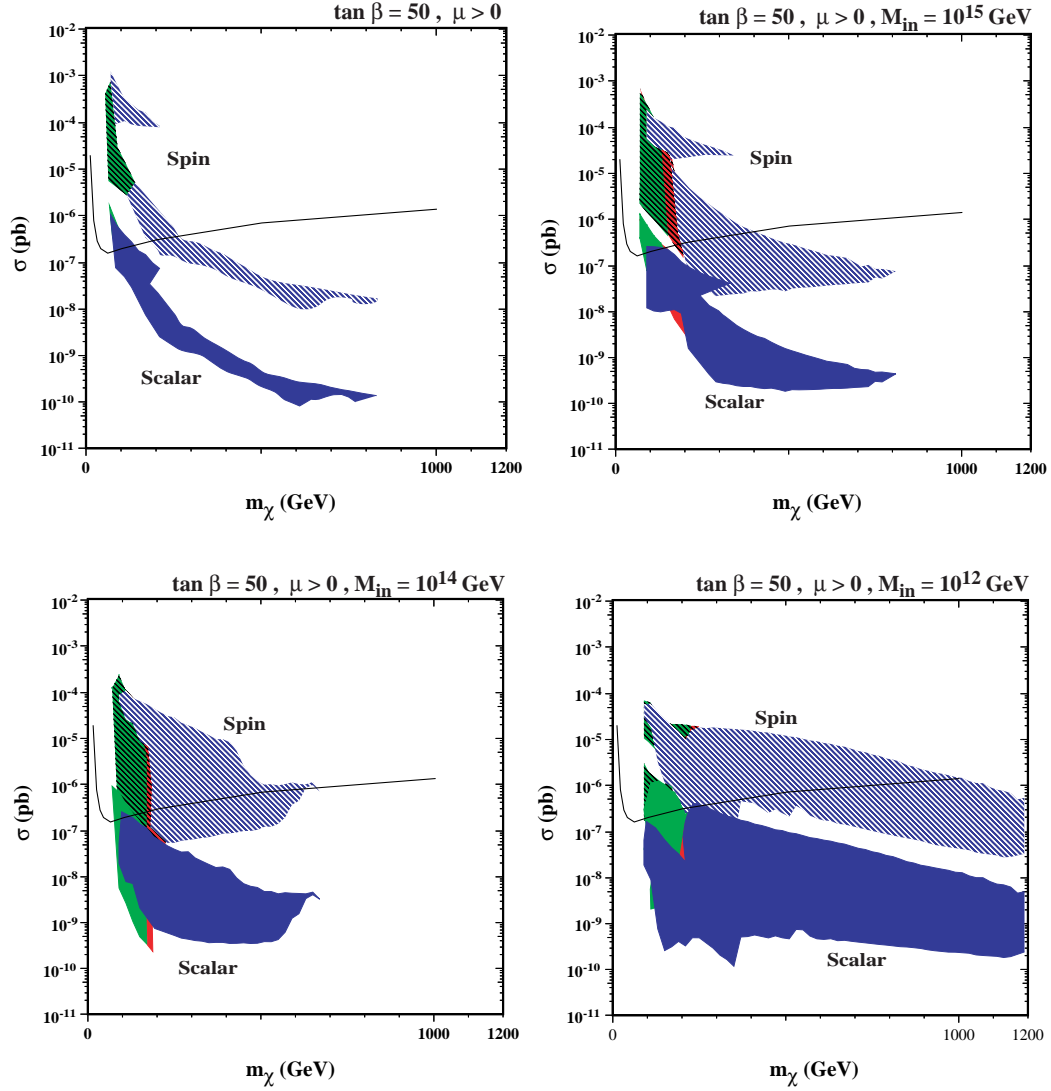


Figure 8: Neutralino-nucleon cross sections as a function of neutralino mass for  $\tan \beta = 50$  and  $A_0 = 0$  but with different values of  $M_{in}$ . (a)  $M_{in} = M_{GUT} \approx 2 \times 10^{16} \text{ GeV}$ , (b)  $M_{in} = 10^{15} \text{ GeV}$ , (c)  $M_{in} = 10^{14} \text{ GeV}$  and (d)  $M_{in} = 10^{12} \text{ GeV}$ .



condition. In fact, for the portion of the  $(m_{1/2}, m_0)$  plane shown in Fig. 2, the focus-point region extends to larger  $m_\chi$  than the coannihilation strip. The two regions are seen as merged in panel (b-d).

As we proceed to panel (c), most of the  $(m_{1/2}, m_0)$  plane results in a relic density of neutralinos that is within or below the cosmologically-preferred range. As a result, there is a uniform distribution of possible cross sections up to  $m_\chi \approx 650$  GeV. The upper boundaries of the scalar and spin-dependent cross sections in panel (c) come from regions in the plane where the relic density is largest and  $m_0$  is lowest, i.e., from the WMAP-preferred regions found at low  $m_0$ . The continuous WMAP region that extends from the  $\tilde{\tau}$ -LSP boundary to larger  $m_0$  and  $m_{1/2}$  is responsible for this uniform upper limit for the cross sections for  $m_\chi \lesssim 650$  GeV. Near  $m_{1/2} = 1100$  GeV, however, a new region of preferred relic density emerges at lower  $m_0$ , leading to a bump in the neutralino-nucleon cross sections that extends to the largest values of  $m_\chi$  considered here.

This same behavior is observed in panel (d), where  $M_{in} = 10^{10}$  GeV. The relic density of neutralinos falls within the WMAP range only in a small region of the  $(m_{1/2}, m_0)$  plane with  $m_{1/2} > 1700$  GeV and is too small elsewhere, but similar increases and decreases in the relic density where different annihilation channels dominate are evident. We also point out that, since the relic density is lower than the WMAP range over most of the plane for  $M_{in} = 10^{12}$  and  $10^{10}$  GeV, we clearly see the maximum weak-scale value of  $m_\chi$ , which corresponds to  $m_{1/2} = 2000$  GeV, decrease between panel (c) and panel (d). For  $M_{in} < 10^{12}$  GeV, the LSP becomes Higgsino-like, with  $m_\chi \sim \mu$  and  $\mu$  decreasing rapidly as  $M_{in}$  is lowered, as discussed in Section 2. For  $\tan \beta = 10$ , the cross sections excluded by CDMS come only from points in the  $(m_{1/2}, m_0)$  plane that also fail the relaxed LEP Higgs constraint.

In Figure 8 we show the neutralino-nucleon cross sections for  $\tan \beta = 50$  with  $M_{in} = M_{GUT}, 10^{15}, 10^{14}$  and  $10^{12}$  GeV. Although the cosmologically-preferred regions of the  $(m_{1/2}, m_0)$  plane are somewhat different from those for  $\tan \beta = 10$ , the plots in Fig. 8 look qualitatively similar to those in Fig. 7. In panel (a) there is a clear separation between the cross sections from the focus-point region and those from the coannihilation strip and the beginning of the rapid-annihilation funnel. Since the funnel region of acceptable relic density pictured in panel (a) of Fig. 4 extends to  $m_{1/2} \approx 1850$  GeV, we find values of the cross sections out to  $m_\chi \approx 850$  GeV. We note that some of the scalar cross sections for  $m_\chi \lesssim 200$  GeV that pass all other constraints outlined above have been excluded by CDMS.

In panel (b), where  $M_{in} = 10^{15}$  GeV, the two regions are still distinct. The lower bulk of cross sections comes now from points inside the fully-developed rapid-annihilation funnel, seen in panel (c) of Fig. 4. Again, we note that had we extended our analysis to larger values of  $m_{1/2}$  and  $m_0$ , acceptable cross sections would be found also at larger  $m_\chi$ .

When  $M_{in} = 10^{14}$  GeV, shown in panel (c), the upper funnel wall has passed through the focus point, and only the lower funnel wall remains. Regions to the left of this wall in the  $(m_{1/2}, m_0)$  plane are essentially inside the funnel and have a very low relic density of neutralinos, whereas the relic density is too large to the right of the wall. Consequently, we see in panel (c) that, at low  $m_\chi$ , the scalar and spin-dependent cross sections span several orders of magnitude.

As in the case when  $\tan \beta = 10$ , at low  $M_{in}$  the relic density of neutralinos falls within

or below the WMAP range over all of the  $(m_{1/2}, m_0)$  plane, so none of the plane is excluded by the constraint on the relic density. This is the case in Panel (d), where  $M_{in} = 10^{12}$  GeV. The situation remains unchanged as  $M_{in}$  is further decreased.

We note that the scalar cross sections are generally larger at large  $\tan\beta$ . In fact, some of these cross sections are already excluded by ZEPLIN-II as well as CDMS II, which both probe WIMP-nucleon scalar cross sections as low as a few  $\times 10^{-7}$  pb [51, 53]. A sensitivity of  $10^{-9}$  pb for  $M_\chi \approx 100$  GeV is expected for SuperCDMS Phase A with seven towers deployed [54]. Many direct dark-matter search experiments plan to use Xenon or Argon as an alternative target material for which the sensitivity scales linearly with the detector mass. The Argon Dark Matter experiment (ArDM) expects to probe spin-independent cross sections as low as  $10^{-10}$  pb with a one-tonne detector operating for one year [55]. Results from direct detection experiments will provide a useful complement to searches for SUSY signatures at colliders.

## 6 Summary

We have examined the impact of lowering the scale of unification of the soft supersymmetry-breaking parameters of the CMSSM on phenomenological, collider and cosmological constraints. In order to carry out this study, we accounted for coannihilations involving the three lightest neutralinos, the lighter chargino, and relevant sleptons and squarks. We explored  $\tan\beta = 10$  and  $\tan\beta = 50$ ,  $A_0 \neq 0$ , and a specific case similar to those found in mirage-mediation models. Intermediate unification scales result in the appearance of a rapid-annihilation funnel even at low  $\tan\beta$ , and the merging of this funnel and the focus-point region as  $M_{in}$  decreases. As the unification scale is lowered below a critical value dependent on  $\tan\beta$  and other factors, the relic density of neutralinos becomes too low to account fully for the required relic density of cold dark matter over all or nearly all of the  $(m_{1/2}, m_0)$  plane. These values of  $M_{in}$  are disfavored in the sense that there must be another source of astrophysical cold dark matter in the universe.

We have also presented the neutralino-nucleon cross sections for several values of  $M_{in}$  at  $\tan\beta = 10$  and  $\tan\beta = 50$ . We find that the spin-independent neutralino-nucleon cross sections for regions of parameter space favored by cosmology are beginning to be excluded by CDMS and other direct detection WIMP searches, although viable cross sections span several orders of magnitude. We look forward to stronger limits on the spin-independent cross sections as direct-detection WIMP searches become more sensitive in the near future.

The analysis in this paper has shown that lowering the scale of unification in even the simplest CMSSM model may alter significantly the phenomenological expectations for both collider and non-collider experiments. It has also revealed novel effects in the calculation of the relic neutralino density, such as the importance of multi-channel neutralino and chargino coannihilation processes. However, we have done little more than scratch the surface of possibilities since, for example, we have not considered in detail scenarios with different values of  $A_0$ , let alone non-CMSSM scenarios or more realistic mirage-mediation models. Another interesting and important question for the future is the accuracy with which the effective unification scale could be estimated on the basis of future collider experiments. We

hope that this work will trigger future studies of these and other related issues.

## Acknowledgments

The work of K.A.O. and P.S. was supported in part by DOE grant DE-FG02-94ER-40823.

## A Neutralino and Chargino Coannihilations

In most standard CMSSM scenarios, the LSP is a bino-like neutralino in many of the regions of parameter space relevant to cosmology, possibly with a significant Higgsino admixture. When the relic density falls near the range favoured by WMAP and other measurements, the neutralinos are typically not degenerate, and therefore there is no opportunity for coannihilations of the LSP with other neutralinos, or with charginos, to bring the relic density down into the range preferred by cosmology. The only case in which it is necessary to include coannihilations involving neutralinos and charginos occurs when the neutralino LSP is Higgsino-like, which arises when  $\mu < M_1$ , a situation that may arise at large  $m_0$  in the focus-point region of the GUT-scale CMSSM<sup>10</sup>. In such a case it is possible for the lightest and second-lightest neutralinos to be degenerate with each other and with the lightest chargino. Thus, at large  $m_0$  and small  $m_{1/2}$  in the GUT-scale CMSSM, coannihilations between the lightest and second lightest neutralinos and with charginos must be included<sup>11</sup>.

In GUT-less scenarios, the lightest neutralino becomes Higgsino-like at low  $M_{in}$ , as discussed in Section 2, so it is necessary to include coannihilations involving the two lightest neutralinos and the lightest chargino as discussed above. However, there is also a region of parameter space where additional coannihilations become significant. When the LSP is mixed and nearly degenerate with the second lightest neutralino and the lightest chargino, in some circumstances the third-lightest neutralino may also be nearly degenerate.

In panels (a) and (b) of Figure 9 we show the masses of all neutralinos and charginos as functions of  $M_{in}$  for two different points in the  $(m_{1/2}, m_0)$  plane. We recall from the discussion in Section 2 that the slope of the curve describing the LSP mass is an indication of its composition: when the neutralino mass increases as  $M_{in}$  decreases, it is gaugino-like, and when it decreases as  $M_{in}$  decreases, tracking  $|\mu|$ , it is Higgsino-like. Panels (a) and (b) show that the masses of the LSP, the second lightest neutralino and the chargino are nearly degenerate when the LSP is Higgsino-like, indicating the necessity of including coannihilations involving all three states. Moreover, just at the point where the LSP changes from bino-like to Higgsino-like, the mass of the third-lightest neutralino dips down near the masses of the two lighter neutralinos and the chargino. Panels (c) and (d) compare the masses of the neutralinos and charginos as functions of  $m_0$  for the CMSSM case with GUT-scale universality and  $M_{in} = 3 \times 10^{11}$  GeV for fixed  $m_{1/2} = 1000$  GeV. One can see in panel (c) that, for the GUT-scale case, there is no degeneracy of the LSP with other neutralinos

---

<sup>10</sup>This situation may also occur in some models with non-universal Higgs masses.

<sup>11</sup>It should be noted that  $\tilde{\tau}$ - $\chi$  coannihilations are known to be of general importance in the CMSSM, since they give rise to the so-called coannihilation strip.

or charginos. The LSP is strongly bino-like, and therefore its mass is related to  $m_{1/2}$ , as in (2), with only a very weak dependence on  $m_0$  through higher-order corrections. The same scenario is shown in panel (d) for  $M_{in} = 3 \times 10^{11}$  GeV. In this case, however, we see that mass degeneracies are apparent over a wide range of values of  $m_0$ .

For some values of  $M_{in}$ , the near-degeneracy of the third-lightest neutralino with lighter neutralinos and the chargino occurs precisely where the relic density of neutralinos is near the cosmologically preferred value. For example, for  $M_{in} = 10^{12}$  GeV and  $\tan\beta = 10$ , the shape and location of the WMAP strip running through (1500, 1000) GeV can shift by as much as 200 GeV in  $m_0$  if coannihilations are not properly included.

Thus, the calculations of the coannihilation processes that previously were included for the second-lightest neutralino have here been calculated also for the third-lightest neutralino, including those of  $\chi_2$  with  $\chi_3$ . Table 1 shows the initial states for all the calculated annihilations and coannihilations of neutralinos and charginos used in the analysis here. In addition to those outlined below, coannihilations of all these neutralino and chargino species with sfermions were calculated, as well as the corresponding sfermion-antisfermion annihilation processes.

$\chi_1\chi_1$	$\chi_1\chi_2$	$\chi_1\chi_+$
$\chi_2\chi_2$	$\chi_2\chi_3$	$\chi_2\chi_+$
$\chi_3\chi_3$	$\chi_3\chi_1$	$\chi_3\chi_+$
	$\chi_+\chi_-$	

Table 1: *Initial states of interactions included here in the calculation of the relic cold dark matter density, where  $\chi_1$  is the LSP and  $\chi_{2(3)}$  is the second (third) -lightest neutralino.*

As noted in the main text, we take the opportunity in this paper to improve on our previous treatment of the rapid-annihilation region and to correct certain coding inaccuracies which, however, have no visible effects on the results we present.

## References

- [1] E. Witten, Nucl. Phys. B **188** (1981) 513; N. Sakai, Z. Phys. C **11** (1981) 153; S. Dimopoulos and H. Georgi, Nucl. Phys. B **193** (1981) 150; R. K. Kaul and P. Majumdar, Nucl. Phys. B **199** (1982) 36.
- [2] J. R. Ellis, S. Kelley and D. V. Nanopoulos, Phys. Lett. B **260** (1991) 131; U. Amaldi, W. de Boer and H. Furstenuau, Phys. Lett. B **260** (1991) 447; P. Langacker and M. x. Luo, Phys. Rev. D **44** (1991) 817; C. Giunti, C. W. Kim and U. W. Lee, Mod. Phys. Lett. A **6** (1991) 1745.
- [3] J. R. Ellis, G. Ridolfi and F. Zwirner, Phys. Lett. B **257** (1991) 83; Phys. Lett. B **262** (1991) 477; A. Yamada, Phys. Lett. B **263**, 233 (1991); M. Drees and M. M. Nojiri, Phys. Rev. D **45** (1992) 2482; P. H. Chankowski, S. Pokorski and J. Rosiek,

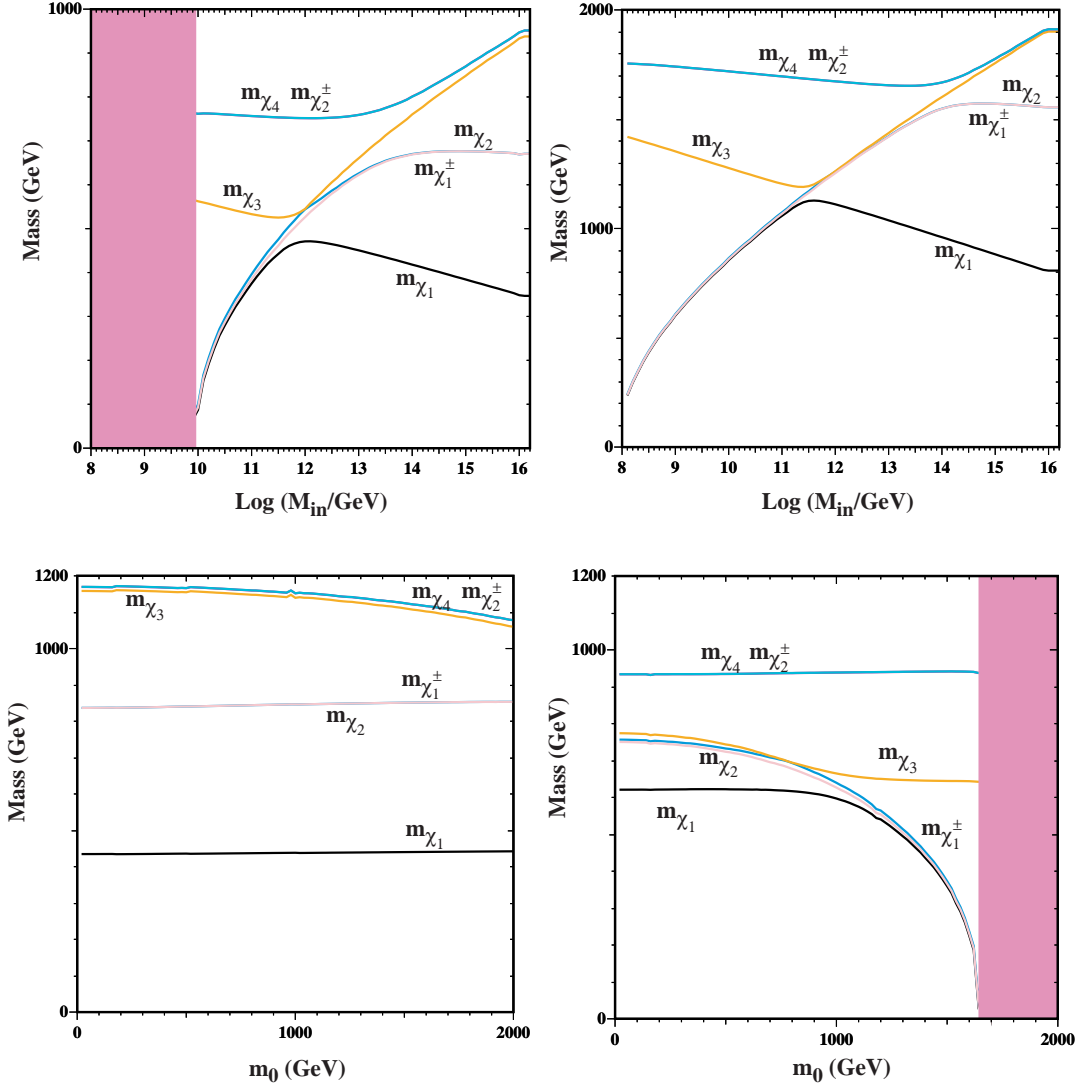


Figure 9: Panels (a) and (b) show the neutralino and chargino masses as functions of  $M_{in}$  for the points  $(m_{1/2}, m_0) = (800, 1000)$  and  $(1800, 1000)$  GeV, respectively. The bottom two panels show the neutralino and chargino masses as functions of  $m_0$  with  $m_{1/2} = 1000$  GeV for (c) the GUT-scale CMSSM case and (d) the GUT-less case with  $M_{in} = 3 \times 10^{11}$  GeV.

- Phys. Lett. B **274** (1992) 191; Phys. Lett. B **286** (1992) 307; A. Dabelstein, Z. Phys. C **67** (1995) 495 [arXiv:hep-ph/9409375]; M. Carena, J. R. Ellis, A. Pilaftsis and C. E. M. Wagner, Nucl. Phys. B **586** (2000) 92 [arXiv:hep-ph/0003180]; A. Katsikatsou, A. B. Lahanas, D. V. Nanopoulos and V. C. Spanos, Phys. Lett. B **501** (2001) 69 [arXiv:hep-ph/0011370].
- [4] J. Ellis, J.S. Hagelin, D.V. Nanopoulos, K.A. Olive and M. Srednicki, Nucl. Phys. B **238** (1984) 453; see also H. Goldberg, Phys. Rev. Lett. **50** (1983) 1419.
- [5] For reviews, see: H. P. Nilles, Phys. Rep. **110** (1984) 1; A. Brignole, L. E. Ibanez and C. Munoz, arXiv:hep-ph/9707209, published in *Perspectives on supersymmetry*, ed. G. L. Kane, pp. 125-148.
- [6] For a review see e.g. H. E. Haber and G. L. Kane, Phys. Rept. **117** (1985) 75.
- [7] M. Drees and M. M. Nojiri, Phys. Rev. D **47** (1993) 376 [arXiv:hep-ph/9207234]; H. Baer and M. Brhlik, Phys. Rev. D **53** (1996) 597 [arXiv:hep-ph/9508321]; J. R. Ellis, T. Falk, K. A. Olive and M. Schmitt, Phys. Lett. B **388** (1996) 97 [arXiv:hep-ph/9607292]; Phys. Lett. B **413** (1997) 355 [arXiv:hep-ph/9705444]; J. R. Ellis, T. Falk, G. Ganis and K. A. Olive, Phys. Rev. D **62** (2000) 075010 [arXiv:hep-ph/0004169]; V. D. Barger and C. Kao, Phys. Rev. D **57** (1998) 3131 [arXiv:hep-ph/9704403].
- [8] J. R. Ellis, T. Falk, G. Ganis, K. A. Olive and M. Schmitt, Phys. Rev. D **58** (1998) 095002 [arXiv:hep-ph/9801445];
- [9] J. R. Ellis, T. Falk, G. Ganis, K. A. Olive and M. Srednicki, Phys. Lett. B **510** (2001) 236 [arXiv:hep-ph/0102098].
- [10] V. D. Barger and C. Kao, Phys. Lett. B **518** (2001) 117 [arXiv:hep-ph/0106189]; L. Roszkowski, R. Ruiz de Austri and T. Nihei, JHEP **0108** (2001) 024 [arXiv:hep-ph/0106334]; A. B. Lahanas and V. C. Spanos, Eur. Phys. J. C **23** (2002) 185 [arXiv:hep-ph/0106345]; A. Djouadi, M. Drees and J. L. Kneur, JHEP **0108** (2001) 055 [arXiv:hep-ph/0107316]; U. Chattopadhyay, A. Corsetti and P. Nath, Phys. Rev. D **66** (2002) 035003 [arXiv:hep-ph/0201001]; J. R. Ellis, K. A. Olive and Y. Santoso, New Jour. Phys. **4** (2002) 32 [arXiv:hep-ph/0202110]; H. Baer, C. Balazs, A. Belyaev, J. K. Mizukoshi, X. Tata and Y. Wang, JHEP **0207** (2002) 050 [arXiv:hep-ph/0205325]; R. Arnowitt and B. Dutta, arXiv:hep-ph/0211417.
- [11] J. R. Ellis, K. A. Olive, Y. Santoso and V. C. Spanos, Phys. Lett. B **565** (2003) 176 [arXiv:hep-ph/0303043]; H. Baer and C. Balazs, arXiv:hep-ph/0303114; A. B. Lahanas and D. V. Nanopoulos, arXiv:hep-ph/0303130; U. Chattopadhyay, A. Corsetti and P. Nath, arXiv:hep-ph/0303201; C. Munoz, hep-ph/0309346.
- [12] J. R. Ellis, K. A. Olive, Y. Santoso and V. C. Spanos, Phys. Rev. D **69** (2004) 095004 [arXiv:hep-ph/0310356]; B. Allanach and C. Lester, *Phys. Rev. D* **73** (2006) 015013, hep-ph/0507283; B. Allanach, hep-ph/0601089; R. de Austri, R. Trotta and

- L. Roszkowski, hep-ph/0602028; J. Ellis, S. Heinemeyer, K. A. Olive and G. Weiglein, arXiv:hep-ph/0602220.
- [13] J. Ellis, S. Heinemeyer, K. Olive and G. Weiglein, *JHEP* **0502** 013, hep-ph/0411216;
- [14] A. Corsetti and P. Nath, Phys. Rev. D **64** (2001) 125010 [arXiv:hep-ph/0003186]; R. Arnowitt, B. Dutta and Y. Santoso, Nucl. Phys. B **606** (2001) 59 [arXiv:hep-ph/0102181]; D. G. Cerdeno, E. Gabrielli, S. Khalil, C. Munoz and E. Torrente-Lujan, Nucl. Phys. B **603** (2001) 231 [arXiv:hep-ph/0102270].
- [15] J. Ellis, K. A. Olive and P. Sandick, Phys. Lett. B **642** (2006) 389 [arXiv:hep-ph/0607002].
- [16] N. Polonsky and A. Pomarol, Phys. Rev. D **51** (1995) 6532 [arXiv:hep-ph/9410231].
- [17] K. Choi, A. Falkowski, H. P. Nilles, M. Olechowski and S. Pokorski, *JHEP* **0411** (2004) 076 [arXiv:hep-th/0411066]; K. Choi, A. Falkowski, H. P. Nilles and M. Olechowski, Nucl. Phys. B **718** (2005) 113 [arXiv:hep-th/0503216]; K. Choi, K. S. Jeong and K. i. Okumura, *JHEP* **0509** (2005) 039 [arXiv:hep-ph/0504037]; M. Endo, M. Yamaguchi and K. Yoshioka, Phys. Rev. D **72** (2005) 015004 [arXiv:hep-ph/0504036]; A. Falkowski, O. Lebedev and Y. Mambrini, *JHEP* **0511** (2005) 034 [arXiv:hep-ph/0507110]; R. Kitano and Y. Nomura, Phys. Lett. B **631** (2005) 58 [arXiv:hep-ph/0509039]; R. Kitano and Y. Nomura, Phys. Rev. D **73** (2006) 095004 [arXiv:hep-ph/0602096]; K. Kawagoe and M. M. Nojiri, [arXiv:hep-ph/0606104]; H. Baer, E.-K. Park, X. Tata and T. T. Wang, *JHEP* **0608** (2006) 041 [arXiv:hep-ph/0604253]; J. P. Conlon, C. H. Kom, K. Suruliz, B. C. Allanach and F. Quevedo, arXiv:0704.3403.
- [18] H. Itoh, N. Okada and T. Yamashita, arXiv:hep-ph/0606156.
- [19] S. Kachru, R. Kallosh, A. Linde and S. P. Trivedi, Phys. Rev. D **68** (2003) 046005 [arXiv:hep-th/0301240].
- [20] D. N. Spergel *et al.*, [arXiv:astro-ph/0603449].
- [21] J. R. Ellis, T. Falk and K. A. Olive, Phys. Lett. B **444** (1998) 367 [arXiv:hep-ph/9810360]; J. R. Ellis, T. Falk, K. A. Olive and M. Srednicki, *Astropart. Phys.* **13** (2000) 181 [Erratum-ibid. **15** (2001) 413] [arXiv:hep-ph/9905481]; R. Arnowitt, B. Dutta and Y. Santoso, Nucl. Phys. B **606** (2001) 59 [arXiv:hep-ph/0102181]; M. E. Gómez, G. Lazarides and C. Pallis, Phys. Rev. D **D61** (2000) 123512 [arXiv:hep-ph/9907261]; Phys. Lett. **B487** (2000) 313 [arXiv:hep-ph/0004028]; Nucl. Phys. B **B638** (2002) 165 [arXiv:hep-ph/0203131]; T. Nihei, L. Roszkowski and R. Ruiz de Austri, *JHEP* **0207** (2002) 024 [arXiv:hep-ph/0206266].
- [22] H. Baer and M. Brhlik, Phys. Rev. D **53** (1996) 597 [arXiv:hep-ph/9508321]; H. Baer, M. Brhlik, M. A. Diaz, J. Ferrandis, P. Mercadante, P. Quintana and X. Tata, Phys.

- Rev. D **63** (2001) 015007 [arXiv:hep-ph/0005027]; A. B. Lahanas and V. C. Spanos, Eur. Phys. J. C **23** (2002) 185 [arXiv:hep-ph/0106345].
- [23] J. L. Feng, K. T. Matchev and T. Moroi, Phys. Rev. Lett. **84** (2000) 2322; J. L. Feng, K. T. Matchev and T. Moroi, Phys. Rev. **D61** (2000) 075005; J. L. Feng, K. T. Matchev and F. Wilczek, Phys. Lett. **B482** (2000) 388.
- [24] Joint LEP 2 Supersymmetry Working Group, *Combined LEP Chargino Results up to 208 GeV*, [http://lepsusy.web.cern.ch/lepsusy/www/inos\\_moriond01/charginos\\_pub.html](http://lepsusy.web.cern.ch/lepsusy/www/inos_moriond01/charginos_pub.html).
- [25] LEP Higgs Working Group for Higgs boson searches, OPAL Collaboration, ALEPH Collaboration, DELPHI Collaboration and L3 Collaboration, Phys. Lett. B **565** (2003) 61 [arXiv:hep-ex/0306033]. *Search for neutral Higgs bosons at LEP*, paper submitted to ICHEP04, Beijing, LHWG-NOTE-2004-01, ALEPH-2004-008, DELPHI-2004-042, L3-NOTE-2820, OPAL-TN-744, [http://lephiggs.web.cern.ch/LEPHIGGS/papers/August2004\\_MSSM/index.html](http://lephiggs.web.cern.ch/LEPHIGGS/papers/August2004_MSSM/index.html).
- [26] Tevatron Electroweak Working Group, *Combination of CDF and D0 results on the mass of the top quark*, arXiv:hep-ex/0603039.
- [27] S. Heinemeyer, W. Hollik and G. Weiglein, *Comput. Phys. Commun.* **124** (2000) 76 [arXiv:hep-ph/9812320]; S. Heinemeyer, W. Hollik and G. Weiglein, *Eur. Phys. J. C* **9** (1999) 343 [arXiv:hep-ph/9812472].
- [28] G. W. Bennett *et al.* [Muon g-2 Collaboration], Phys. Rev. Lett. **92** (2004) 161802 [arXiv:hep-ex/0401008]; M. Davier, S. Eidelman, A. Hocker and Z. Zhang, Eur. Phys. J. C **31** (2003) 503 [arXiv:hep-ph/0308213]; K. Hagiwara, A. D. Martin, D. Nomura and T. Teubner, arXiv:hep-ph/0312250; J. F. de Trocóniz and F. J. Ynduráin, arXiv:hep-ph/0402285; K. Melnikov and A. Vainshtein, arXiv:hep-ph/0312226; M. Passera, arXiv:hep-ph/0411168; K. Hagiwara, A. D. Martin, D. Nomura and T. Teubner, arXiv:hep-ph/0611102.
- [29] M. Davier, arXiv:hep-ph/0701163; F. Jegerlehner, arXiv:hep-ph/0703125; J. P. Miller, E. de Rafael and B. L. Roberts, arXiv:hep-ph/0703049.
- [30] S. Eidelman, talk given at the ICHEP06, Moscow, July 2006, see: [ic hep06.jinr.ru/reports/333\\_6s1\\_9p30\\_Eidelman.pdf](http://ic hep06.jinr.ru/reports/333_6s1_9p30_Eidelman.pdf) .
- [31] M. Ciuchini, G. Degrossi, P. Gambino and G. F. Giudice, Nucl. Phys. B **527** (1998) 21 [arXiv:hep-ph/9710335]; Nucl. Phys. B **534** (1998) 3 [arXiv:hep-ph/9806308]; C. Degrossi, P. Gambino and G. F. Giudice, JHEP **0012** (2000) 009 [arXiv:hep-ph/0009337]; M. Carena, D. Garcia, U. Nierste and C. E. Wagner, Phys. Lett. B **499** (2001) 141 [arXiv:hep-ph/0010003]; P. Gambino and M. Misiak, Nucl. Phys. B **611** (2001) 338; D. A. Demir and K. A. Olive, Phys. Rev. D **65** (2002) 034007 [arXiv:hep-ph/0107329]; F. Borzumati, C. Greub and Y. Yamada, Phys. Rev. D **69**



- (2004) 055005 [arXiv:hep-ph/0311151]; T. Hurth, *Rev. Mod. Phys.* **75** (2003) 1159 [arXiv:hep-ph/0212304].
- [32] M. Misiak *et al.*, *Phys. Rev. Lett.* **98** (2007) 022002, hep-ph/0609232.
- [33] S. Chen *et al.* [CLEO Collaboration], *Phys. Rev. Lett.* **87** (2001) 251807 [arXiv:hep-ex/0108032]; P. Koppenburg *et al.* [Belle Collaboration], *Phys. Rev. Lett.* **93** (2004) 061803 [arXiv:hep-ex/0403004]. B. Aubert *et al.* [BaBar Collaboration], arXiv:hep-ex/0207076.
- [34] E. Barberio *et al.* [Heavy Flavor Averaging Group (HFAG)], arXiv:hep-ex/0603003.
- [35] A. Dedes, H. K. Dreiner and U. Nierste, *Phys. Rev. Lett.* **87** (2001) 251804 [arXiv:hep-ph/0108037]; R. Arnowitt, B. Dutta, T. Kamon and M. Tanaka, *Phys. Lett. B* **538** (2002) 121 [arXiv:hep-ph/0203069]; S. Baek, P. Ko and W. Y. Song, *Phys. Rev. Lett.* **89** (2002) 271801 [arXiv:hep-ph/0205259]; C. S. Huang and X. H. Wu, *Nucl. Phys. B* **657** (2003) 304 [arXiv:hep-ph/0212220]; S. Baek, Y. G. Kim and P. Ko, *JHEP* **0502** (2005) 067 [arXiv:hep-ph/0406033]; H. Baer, C. Balazs, A. Belyaev, J. K. Mizukoshi, X. Tata and Y. Wang, *JHEP* **0207** (2002) 050 [arXiv:hep-ph/0205325].
- [36] J. R. Ellis, K. A. Olive and V. C. Spanos, *Phys. Lett. B* **624** (2005) 47 [arXiv:hep-ph/0504196].
- [37] F. Abe *et al.* [CDF Collaboration], *Phys. Rev. D* **57** (1998) 3811;  
D. Acosta *et al.* [CDF Collaboration], *Phys. Rev. Lett.* **93** (2004) 032001, hep-ex/0403032;  
V. Abazov *et al.* [D0 Collaboration], *Phys. Rev. Lett.* **94** (2005) 071802, hep-ex/0410039;  
D0 Collaboration, D0note, 4733-CONF, see:  
[www-d0.fnal.gov/Run2Physics/WWW/results/prelim/B/B21/B21.pdf](http://www-d0.fnal.gov/Run2Physics/WWW/results/prelim/B/B21/B21.pdf) ;  
M. Herndon [CDF and D0 Collaborations], FERMILAB-CONF-04-391-E. Published Proceedings 32nd International Conference on High-Energy Physics (ICHEP 04), Beijing, China, August 16-22, 2004;  
CDF Collaboration, CDF note 7670, see:  
[www-cdf.fnal.gov/physics/new/bottom/050407.blessed-bsmumu](http://www-cdf.fnal.gov/physics/new/bottom/050407.blessed-bsmumu) .
- [38] K. Griest and D. Seckel, *Phys. Rev. D* **43** (1991) 3191; S. Mizuta and M. Yamaguchi, *Phys. Lett.* **B298** (1993) 120.
- [39] J. R. Ellis, K. A. Olive and Y. Santoso, *Astropart. Phys.* **18** 395 (2003) [arXiv:hep-ph/0112113]; C. Boehm, A. Djouadi and M. Drees, *Phys. Rev. D* **62**, 035012 (2000) [arXiv:hep-ph/9911496]; J. L. Diaz-Cruz, J. Ellis, K. A. Olive and Y. Santoso, [arXiv:hep-ph/0701229].
- [40] D. S. Akerib *et al.* [CDMS Collaboration], *Phys. Rev. Lett.* **93** (2004) 211301 [arXiv:astro-ph/0405033].

- [41] K. Griest, Phys. Rev. D **38** (1988) 2357; J. Ellis and R. Flores, Nucl. Phys. B **307** (1988) 883; R. Barbieri, M. Frigeni and G. Giudice, Nucl. Phys. B **313**(1989) 725; R. Flores, K. A. Olive and M. Srednicki, Phys. Lett. B **237**(1990) 72; J. Ellis and R. Flores, Phys. Lett. B **263** (1991) 259; J. Ellis and R. Flores, Phys. Lett. B **300** (1993) 175; M. Drees and M. M. Nojiri, Phys. Rev. D **48** (1993) 3483; V. Bednyakov, H. V. Klapdor-Kleingrothaus and S. Kovalenko, Phys. Rev. D **50** (1994) 7128; R. Arnowitt and P. Nath, Phys. Rev. D **54** (1996) 2374 [arXiv:hep-ph/9509260]; L. Bergstrom and P. Gondolo, Astropart. Phys. **5**, 263 (1996) [arXiv:hep-ph/9510252]; H. Baer and M. Brhlik, Phys. Rev. D **57** (1998) 567 [arXiv:hep-ph/9706509]; A. Corsetti and P. Nath, Phys. Rev. D **64** (2001) 125010 [arXiv:hep-ph/0003186].
- [42] E. Accomando, R. Arnowitt, B. Dutta and Y. Santoso, Nucl. Phys. B **585** (2000) 124 [arXiv:hep-ph/0001019]; R. Arnowitt, B. Dutta and Y. Santoso, arXiv:hep-ph/0005154.
- [43] J. Ellis, A. Ferstl and K. A. Olive, Phys. Lett. B **481** (2000) 304 [arXiv:hep-ph/0001005]; J. Ellis, A. Ferstl and K. A. Olive, Phys. Rev. D **63** (2001) 065016 [arXiv:hep-ph/0007113]; J. R. Ellis, A. Ferstl and K. A. Olive, Phys. Lett. B **532** (2002) 318 [arXiv:hep-ph/0111064].
- [44] J. R. Ellis, A. Ferstl, K. A. Olive and Y. Santoso, Phys. Rev. D **67** (2003) 123502 [arXiv:hep-ph/0302032].
- [45] J. R. Ellis, J. L. Feng, A. Ferstl, K. T. Matchev and K. A. Olive, Eur. Phys. J. C **24** (2002) 311 [arXiv:astro-ph/0110225].
- [46] For other scattering calculations, see, for example: J. L. Feng, K. T. Matchev and F. Wilczek, Phys. Lett. B **482** (2000) 388 [arXiv:hep-ph/0004043]; M. Drees, Y. G. Kim, T. Kobayashi and M. M. Nojiri, Phys. Rev. D **63** (2001) 115009 [arXiv:hep-ph/0011359]; Y. G. Kim and M. M. Nojiri, arXiv:hep-ph/0104258; A. B. Lahanas, D. V. Nanopoulos and V. C. Spanos, Mod. Phys. Lett. A **16** (2001) 1229 [arXiv:hep-ph/0009065]; A. B. Lahanas, D. V. Nanopoulos and V. C. Spanos, Phys. Lett. B **518** (2001) 94 [arXiv:hep-ph/0107151]; E. A. Baltz and P. Gondolo, Phys. Rev. Lett. **86** (2001) 5004 [arXiv:hep-ph/0102147]; Y. G. Kim, T. Nihei, L. Roszkowski and R. Ruiz de Austri, JHEP **0212** (2002) 034 [arXiv:hep-ph/0208069]; M. E. Gómez and J. D. Vergados, Phys. Lett. B **512** (2001) 252 [arXiv:hep-ph/0012020]; H. Baer, C. Balazs, A. Belyaev and J. O’Farrill, JCAP **0309** (2003) 007 [arXiv:hep-ph/0305191].
- [47] A. Bottino, F. Donato, N. Fornengo and S. Scopel, Phys. Rev. D **59** (1999) 095003 [arXiv:hep-ph/9808456]; Phys. Rev. D **59** (1999) 095004 [arXiv:hep-ph/9808459]; Phys. Rev. D **63** (2001) 125003 [arXiv:hep-ph/0010203]; R. Arnowitt and P. Nath, Phys. Rev. D **60** (1999) 044002 [arXiv:hep-ph/9902237]; R. Arnowitt, B. Dutta and Y. Santoso, Nucl. Phys. B **606** (2001) 59 [arXiv:hep-ph/0102181].
- [48] A. Bottino, F. Donato, N. Fornengo and S. Scopel, Astropart. Phys. **13** (2000) 215 [arXiv:hep-ph/9909228]; Astropart. Phys. **18** (2002) 205 [arXiv:hep-ph/0111229].

- [49] J. R. Ellis, K. A. Olive, Y. Santoso and V. C. Spanos, Phys. Rev. D **71** (2005) 095007 [arXiv:hep-ph/0502001].
- [50] D. G. Cerdeño, S. Khalil and C. Muñoz, [arXiv:hep-ph/0105180].
- [51] D. S. Akerib *et al.* [CDMS Collaboration], Phys. Rev. Lett. **96**, 011302 (2006) [arXiv:astro-ph/0509259].
- [52] H. S. Lee *et al.* [arXiv:0704.0423v1].
- [53] G. J. Alner *et al.* [ZEPLIN II Collaboration], [arXiv:astro-ph/0701858].
- [54] R. W. Schnee *et al.* [SuperCDMS Collaboration], [arXiv:astro-ph/0502435].
- [55] A. Rubbia, J. Phys. Conf. Ser. **39** 129 (2006) [arXiv:hep-ph/0510320].